

Human coronavirus OC43-elicited CD4⁺ T cells protect against SARS-CoV-2 in HLA transgenic mice

Received: 18 August 2023

Accepted: 10 January 2024

Published online: 26 January 2024

 Check for updates

Rúbens Prince dos Santos Alves ¹, Julia Timis¹, Robyn Miller¹, Kristen Valentine¹, Paolla Beatriz Almeida Pinto¹, Andrew Gonzalez¹, Jose Angel Regla-Nava^{1,7}, Erin Maule¹, Michael N. Nguyen ¹, Norazizah Shafee ¹, Sara Landeras-Bueno¹, Eduardo Olmedillas¹, Brett Laffey², Katarzyna Dobaczewska ², Zbigniew Mikulski², Sara McArdle ², Sarah R. Leist ³, Kenneth Kim ⁴, Ralph S. Baric ^{3,5}, Erica Ollmann Saphire ^{1,6}, Annie Elong Ngono ¹ ✉ & Sujan Shresta ¹ ✉

SARS-CoV-2-reactive T cells are detected in some healthy unexposed individuals. Human studies indicate these T cells could be elicited by the common cold coronavirus OC43. To directly test this assumption and define the role of OC43-elicited T cells that are cross-reactive with SARS-CoV-2, we develop a model of sequential infections with OC43 followed by SARS-CoV-2 in HLA-B*0702 and HLA-DRB1*0101 *Ifnar1*^{-/-} transgenic mice. We find that OC43 infection can elicit polyfunctional CD8⁺ and CD4⁺ effector T cells that cross-react with SARS-CoV-2 peptides. Furthermore, pre-exposure to OC43 reduces subsequent SARS-CoV-2 infection and disease in the lung for a short-term in HLA-DRB1*0101 *Ifnar1*^{-/-} transgenic mice, and a longer-term in HLA-B*0702 *Ifnar1*^{-/-} transgenic mice. Depletion of CD4⁺ T cells in HLA-DRB1*0101 *Ifnar1*^{-/-} transgenic mice with prior OC43 exposure results in increased viral burden in the lung but no change in virus-induced lung damage following infection with SARS-CoV-2 (versus CD4⁺ T cell-sufficient mice), demonstrating that the OC43-elicited SARS-CoV-2 cross-reactive T cell-mediated cross-protection against SARS-CoV-2 is partially dependent on CD4⁺ T cells. These findings contribute to our understanding of the origin of pre-existing SARS-CoV-2-reactive T cells and their effects on SARS-CoV-2 clinical outcomes, and also carry implications for development of broadly protective betacoronavirus vaccines.

Severe acute respiratory syndrome coronavirus 2 (SARS-CoV-2) is the causative pathogen of the current coronavirus disease 2019 (COVID-19) pandemic. Despite the deployment of several effective SARS-CoV-2 vaccines, the pandemic has been sustained by the emergence of several variants of concern, including Beta (B.1.351), Delta (B.1.617.2), and Omicron (B.1.1.529), which displayed varying degrees of resistance to neutralizing antibodies acquired naturally or via vaccination^{1–5}. Clinical

manifestations of primary SARS-CoV-2 infection range in severity from asymptomatic or mild/moderate symptoms to respiratory failure, multiorgan dysfunction, and death^{6–11}. While several factors, including age, gender, and comorbidities, are known to impact the clinical outcome of infection^{10,12–17}, little is known about whether and how pre-existing cross-reactive T-cell immunity influences the course of infection.

A full list of affiliations appears at the end of the paper. ✉ e-mail: aelong@lji.org; sujan@lji.org

Several studies have shown that SARS-CoV-2 infection or vaccination can elicit robust CD8⁺ and CD4⁺ T cell responses in humans^{18–26}, and previously unexposed individuals also have functional CD8⁺ and CD4⁺ T cells with reactivity to SARS-CoV-2^{27–32}. This pre-existing T-cell immunity is thought to result from prior exposure to 1 or more of 4 related human coronaviruses (HCoVs): OC43, HKU1, 229E, and NL63. While not yet been formally proven, this assertion is premised on 2 key observations. First, these four HCoVs are collectively responsible for about 15%–30% of common cold infections annually in adults³³, and approximately 50%–90% of the global population are seropositive for at least one of the four viruses³⁴. Second, these 4 HCoVs share roughly 80% genomic sequence identity with SARS-CoV-2³⁵ (Table S1).

Pre-existing cross-reactive T cells have been associated with both protective and pathogenic immunity to SARS-CoV-2. Specifically, cross-reactive CD4⁺ T cells have been associated with enhanced immune responses against SARS-CoV-2 infection and vaccination^{36,37} and the development of severe COVID-19³⁸. In contrast, pre-existing cross-reactive CD8⁺ T cells have been associated with asymptomatic SARS-CoV-2 infection³⁹ and reduced COVID-19 severity and shorter disease duration^{40–42}. There is precedent for pre-existing immunity leading to disparate effects on disease outcomes. For example, exposure to flaviviruses such as dengue and Zika viruses can either protect against or severely exacerbate subsequent infections with a different flavivirus or heterologous serotype^{43–56}. Whether anti-flavivirus immunity is protective or pathogenic depends on multiple variables, including the combination of flaviviruses or serotypes, the source of cross-reactive immunity (antibody, CD8⁺ T cells, CD4⁺ T cells), and the time between primary and subsequent infections^{57–61}. Thus, understanding the nature and effects of pre-existing cross-reactive immunity to SARS-CoV-2 has implications for identifying factors responsible for the disparate clinical outcomes among COVID-19 patients, and designing pan-coronavirus vaccines.

In this study, we investigated the antigen cross-reactivity of pre-existing OC43-elicited T cells and their biological roles during subsequent SARS-CoV-2 infection. Human leukocyte antigen (HLA) is a key determinant of the magnitude, breadth, and specificity of the T cell response in humans. To maintain human relevance, we employed our published transgenic HLA-B*0702 and HLA-DRB1*0101 *Ifnar1*^{-/-} mouse models. HLA-B*0702 and HLA-DRB1*0101 are 2 of the most common human MHC class I and II alleles, being expressed by up to 18% and 13%, respectively, of some populations^{62,63}. Deletion of type I interferon receptors (*Ifnar1*^{-/-}) in these mice permits the study of immunity to viruses that cannot replicate in mice with an intact IFN response. Interestingly, several human cohort studies have observed an association between severe COVID-19 and inborn or acquired deficiency in the type I IFN pathway^{64–70}. For example, autoantibodies against type I IFNs were detected in 20% of patients with severe COVID-19, suggesting that such autoantibodies may be a common source of acquired immune compromise⁶⁴. We previously used HLA-B*0702 and HLA-DRB1*0101 *Ifnar1*^{-/-} mice to demonstrate that CD8⁺ and CD4⁺ T cell responses to flaviviruses mirror those seen in humans with respect to antigen specificities, immunodominance patterns, T cell response kinetics, and the influence of pre-existing cross-reactive immunity in shaping the secondary T cell response and clinical outcomes^{60,71–74}. Thus, with HLA transgenic *Ifnar1*^{-/-} mice, we were able to directly address the questions of whether prior exposure to common cold HCoVs can be a source of cross-reactive SARS-CoV-2 immunity and, if so, how pre-existing cross-reactive immunity may influence the outcome of SARS-CoV-2 infection.

In this work, we first identified human-relevant immunodominant SARS-CoV-2 CD8⁺ and CD4⁺ T cell epitopes in two different contexts: immunization with DNA-based vaccines encoding SARS-CoV-2 spike (S), membrane (M), or nucleocapsid (N) proteins; and infection with SARS-CoV-2. We then established the cross-reactivity of OC43-elicited T cells to SARS-CoV-2 peptides, examined the effect of prior exposure

to OC43 on subsequent SARS-CoV-2 infection and lung disease, and determined the contribution of cross-reactive CD4⁺ T cells to OC43-induced cross-protection. Our results demonstrate that prior exposure to OC43 generates cross-protective immunity that is mediated, at least in part, by CD4⁺ T cells against SARS-CoV-2 infection and lung disease.

Results

Identification of SARS-CoV-2 epitopes recognized by T cells in DNA-vaccinated HLA-B*0702 and HLA-DRB1*0101 *Ifnar1*^{-/-} mice

To investigate CD8⁺ and CD4⁺ T cell responses to SARS-CoV-2 in the context of human HLA alleles, we first identified the major predicted HLA-B*0702- and HLA-DRB1*0101-restricted T cell epitopes in SARS-CoV-2 S, N, and M proteins, which are known to be major CD8⁺ and CD4⁺ T cell targets in infected humans²³. Using the Immune Epitope Database⁷⁵ to identify potentially immunogenic peptides, we selected the top 1% of SARS-CoV-2 S, M, and N peptides predicted to have high-affinity binding to HLA-B*0702 or HLA-DRB1*0101, and obtained 69 class I-restricted epitopes (Table 1) and 42 class II-restricted epitopes (Table 2). Mice from both strains were vaccinated with a DNA-based vaccine encoding SARS-CoV-2 S, M, or N proteins (Figs. 1A, B) on days 0 and 14, and spleens and lungs were collected 7 days later (Fig. 1C). Splenocytes and lung leukocytes were incubated with each peptide (*vs* no-peptide control), and IFN γ -producing peptide-specific T cells were quantified by ELISpot.

Splenocytes from DNA-vaccinated HLA-B*0702 transgenic mice produced significantly higher levels of IFN γ in response to 13 of the 69 peptides (S₆₂₀₋₆₂₉, S₆₇₈₋₆₈₈, S₆₈₀₋₆₈₇, S₆₈₀₋₆₈₈, S₁₀₅₆₋₁₀₆₃, N₆₄₋₇₄, N₆₅₋₇₄, N₆₆₋₇₄, N₆₆₋₇₅, N₆₆₋₇₆, N₁₀₄₋₁₁₃, N₁₀₅₋₁₁₃, and N₁₀₅₋₁₁₄) compared to control cells; lung leukocytes from the same mice showed significantly elevated levels of IFN γ secretion in response to 7 of the 69 peptides (S₁₀₅₆₋₁₀₆₃, N₆₄₋₇₄, N₆₅₋₇₄, N₆₆₋₇₅, N₆₆₋₇₆, N₁₀₄₋₁₁₃, and N₁₀₅₋₁₁₃; Fig. 1D). Of the 7 peptides that induced significant IFN γ responses in both lung leukocytes and splenocytes, the highest response was to the 3 peptides spanning residues 104 to 113 of the N protein (Fig. 1D); this was confirmed by intracellular cytokine staining (ICS) (Fig. S1). In vaccinated HLA-DRB1*0101 mice, 3 of the 42 predicted peptides (S₃₁₅₋₃₂₉, S₉₅₉₋₉₇₃, and M₁₆₅₋₁₇₉) resulted in significant stimulation of IFN γ production by splenocytes, and 2 peptides (S₃₁₅₋₃₂₉ and S₉₉₈₋₁₀₁₂) significantly stimulated a response in lung leukocytes; thus S₃₁₅₋₃₂₉ stimulated splenocytes and lung leukocytes (Fig. 1E). In contrast to the class I-restricted response, none of the N protein-derived peptides stimulated a significant IFN γ response in DNA-vaccinated HLA-DRB1*0101 mice. These data demonstrate that SARS-CoV-2 DNA-based vaccines elicited T-cell responses dominated by recognition of S and N protein-derived peptides in the spleen and lung of HLA-B*0702 *Ifnar1*^{-/-} mice and by S and M protein-derived peptides in HLA-DRB1*0101 *Ifnar1*^{-/-} mice.

SARS-CoV-2 infection elicits effector CD8⁺ and Th1-biased CD4⁺ T cell responses in HLA transgenic *Ifnar1*^{-/-} mice

To determine whether the antigen-specificities of the T cell response elicited by SARS-CoV-2 DNA vaccines and live virus are similar, we infected HLA-DRB1*0101 *Ifnar1*^{-/-} mice with mouse-adapted SARS-CoV-2 MA10 strain⁷⁶ and HLA-B*0702 *Ifnar1*^{-/-} mice with SARS-CoV-2 B.1.351 (Beta), which can replicate in mice without the need for adaptation^{77,78}. Spleens were collected on day 8 post-infection (Fig. 2A), splenocytes were stimulated with select SARS-CoV-2 peptides, immunolabeled for cell surface markers, intracellular cytokines, and the degranulation marker CD107a, and the frequencies of activated (CD44⁺ CD62L⁻) effector CD8⁺ and CD4⁺ T cells were quantified by flow cytometry (Fig. S2).

The CD8⁺ T cell response in B.1.351-infected HLA-B*0702 *Ifnar1*^{-/-} mice was assessed by stimulating splenocytes with the 6 most potent SARS-CoV-2-derived peptides identified by DNA vaccination (S₆₇₈₋₆₈₈, S₁₀₅₆₋₁₀₆₃, N₆₆₋₇₆, N₁₀₄₋₁₁₃, M₁₀₃₋₁₁₂, M₁₆₄₋₁₇₂). While the frequencies of activated IFN γ ⁺, IFN γ ⁺/TNF⁺, IFN γ ⁺/TNF⁺/IL-2⁺, and IFN γ ⁺/CD107a⁺ CD8⁺

Table 1 | Predicted HLA-B*0702-restricted epitopes from SARS-CoV-2 S-, M-, and N-proteins

Protein	Start	End	Length	Sequence	
Spike	24	32	9	LPPAYTNSF	
	38	47	10	YDPKVFRRSSV	
	38	48	11	YDPKVFRRSSVL	
	56	65	10	LPFFSNVTWF	
	207	216	10	HTPINLVRDL	
	208	216	9	TPINLVRDL	
	216	223	8	LPQGFSAL	
	216	226	11	LPQGFSALEPL	
	329	338	10	FPNITNLCPF	
	411	419	9	APGQTGKIA	
	462	472	11	KPFERDISTEI	
	506	515	10	QPYRVVLSF	
	506	513	8	QPYRVVVL	
	526	534	9	GPKKSTNLV	
	588	597	10	TPCSFGGVSV	
	620	629	10	VPVAIHADQL	
	630	638	9	TPTWRVYST	
	678	688	11	TNSPRRARSVA	
	679	688	10	NSPRRARSVA	
	680	688	9	SPRRARSVA	
	680	689	10	SPRRARSVAS	
	680	687	8	SPRRARSV	
	683	692	10	RARSVASQSI	
	691	699	9	SIIAYTMSL	
	713	722	10	AIPTNFTISV	
	714	722	9	IPTNFTISV	
	727	736	10	LPVSMTKTSV	
	811	821	11	KPSKRSFIEDL	
	811	818	8	KPSKRSFI	
	869	877	9	MIAQYTSAL	
	1014	1022	9	RAAEIRASA	
	1052	1061	10	FPQSAPHGVV	
	1052	1062	11	FPQSAPHGVVF	
	1052	1060	9	FPQSAPHGV	
	1056	1063	8	APHGVVFL	
	1089	1097	9	FPREGVFVS	
	1089	1096	8	FPREGVFV	
	1261	1270	10	SEPVLKGVKL	
	Membrane	58	67	10	WPVTLACFVL
		101	109	9	RLFARTRSM
		103	112	10	FARTRSMWSF
		122	129	8	VPLHGTL
131		138	8	RPLLESEL	
131		140	10	RPLLESELVI	
148		156	9	HLRIAGHHL	
164		172	9	LPKEITVAT	
Nucleoprotein		12	21	10	APRITFGGPS
	41	50	10	RPQGLPNNTA	
	45	53	9	LPNNTASWF	
	64	74	11	LKFPQQGVPI	
	65	74	10	KFPQQGVPI	
	66	74	9	FPRQQGVPI	
	66	75	10	FPRQQGVPIIN	
	66	76	11	FPRQQGVPIINT	

Table 1 (continued) | Predicted HLA-B*0702-restricted epitopes from SARS-CoV-2 S-, M-, and N-proteins

Protein	Start	End	Length	Sequence
Spike	66	73	8	FPRQQGVPI
	67	74	8	PRGQQGVPI
	93	101	9	RIRGGDGKM
	104	113	10	LSPRWYFYLL
	105	113	9	SPRWYFYLL
	105	114	10	SPRWYFYLLG
	149	158	10	RNPANNAIV
	150	159	10	NPANNAIVL
	150	158	9	NPANNAIV
	161	171	11	LPQGTTLPKGF
	256	265	10	KKPRQKRTAT
	257	265	9	KPRQKRTAT
	257	267	11	KPRQKRTATKA
	257	264	8	KPRQKRTA
	308	317	10	APSASAFFGM

T cells were significantly increased in response to stimulation with epitope N₁₀₄₋₁₁₃ (vs control), there was no significant expansion in response to the other 5 peptides (Fig. 2B, with the gating strategy represented in Fig. S2A). Thus, vaccination with a SARS-CoV-2 N protein-encoding DNA vaccine and direct infection with B.1.351 elicited effector CD8⁺ T cell response in HLA-B*0702 *Ifnar1*^{-/-} mice that were both directed against the immunodominant epitope N₁₀₄₋₁₁₃. This finding is in agreement with previous reports that SARS-CoV-2 N₁₀₅₋₁₁₃ is the immunodominant epitope in SARS-CoV-2-infected individuals expressing HLA-B*0702^{25,28,79-82}.

As the class II-restricted response to SARS-CoV-2 DNA vaccines was lower in magnitude than the class I-restricted response, we stimulated splenocytes from MA10-infected HLA-DRB1*0101 *Ifnar1*^{-/-} mice with each of the 42 SARS-CoV-2 peptides predicted to be immunogenic in the context of HLA-DRB1*0101, and then analyzed the frequencies of activated CD4⁺ T cells producing IFN γ alone or IFN γ and TNF (Th1 cells), IL-4 (Th2 cells), and IL-17A (Th17 cells) (Fig. 2C, with the gating strategy represented in Fig. S2B). All 42 peptides increased the frequency of IFN γ -producing cells compared with unstimulated control cells, but the increase was significant only in response to 2 peptides: S₉₅₉₋₉₇₃ and N₁₀₇₋₁₂₁. Three peptides expanded multifunctional IFN γ /TNF⁺ CD4⁺ T cells (S₃₁₅₋₃₂₉, S₅₁₂₋₅₂₆, and N₃₂₈₋₃₄₂). In contrast, none of the peptides stimulated CD4⁺ T cell production of IL-4 or IL-17A. Of note, N₁₀₇₋₁₂₁ encompasses most of the immunodominant N₁₀₄₋₁₁₃ CD8⁺ T cell epitope identified in both DNA-vaccinated and SARS-CoV-2-infected HLA-B*0702 *Ifnar1*^{-/-} mice, and S₃₁₅₋₃₂₉ also stimulated splenocytes from the DNA-vaccinated HLA-DRB1*0101 *Ifnar1*^{-/-} mice. These findings demonstrate that the major CD4⁺ T cell response to primary infection with SARS-CoV-2 MA10 in HLA-DRB1*0101 *Ifnar1*^{-/-} mice is Th1-biased, which is consistent with human studies showing that SARS-CoV-2 infection or vaccination elicits CD4⁺ T cells with a Th1-like phenotype^{23,83,84}. Moreover, the agreement between the human studies and our findings in both DNA-vaccinated and SARS-CoV-2-infected HLA transgenic mice further validates these mouse models for investigation of human-relevant CD8⁺ and CD4⁺ T cell responses to SARS-CoV-2.

OC43 infection elicits CD8⁺ T cells with cross-reactivity to SARS-CoV-2 in HLA-B*0702 *Ifnar1*^{-/-} mice

The genomic sequence of SARS-CoV-2 N protein is 29% and 23% identical to the N protein sequences of β -coronaviruses (OC43 and HKU-1) and α -coronaviruses (NL63 and 229E), respectively^{85,86}. To

Table 2 | Predicted HLA-DRB1*0101-restricted epitopes from SARS-CoV-2 S-, M-, and N-proteins

Protein	Start	End	Length	Sequence
Spike	4	18	15	FLVLLPLVSSQCIVNL
	54	68	15	LFLPFFSNVTWFHAI
	62	76	15	VTWFHAIHVSQTNGT
	115	129	15	QSLIVNATNVVIK
	199	213	15	GYFKIYSKHTPINLV
	231	245	15	IGINITRFQTLALH
	236	250	15	TRFQTLALHRSYLT
	264	278	15	AYYVGYLQPRTEFLK
	315	329	15	TSNFRVQPTESIVRF
	344	358	15	ATRFASVYAWNKRRI
	363	377	15	ADYSVLYNSASFSTF
	512	526	15	VLSFELLHAPATVCG
	539	553	15	VNFNFGTLTGTGVL
	692	706	15	IIAYTMSLGAENSV
	758	772	15	SFCTQLNRALTGI
	853	867	15	QKFNGTLVPLPLTD
	869	883	15	MIAQYTSALLAGTIT
	885	899	15	GWTFGAGAALQIPFA
	895	909	15	QIPFAMQMAYRFNGI
	902	916	15	MAYRFNGIGVTQNV
	959	973	15	LNTLVKQLSSNF
	967	981	15	SSNFQAISVLDN
	998	1012	15	TGRLQSLQTYVTQQL
1005	1019	15	QTYVTQQLIRAAEIR	
1010	1024	15	QQLIRAAEIRASANL	
1015	1029	15	AAEIRASANLAATKM	
1044	1058	15	GKGYHLMSPQSA	
Membrane	32	46	15	ICLLQFAYANRNRFL
	60	74	15	VTLACFVLAAYRIN
	71	85	15	YRINWITGGIAIAMA
	91	105	15	MWLSYFIASFRLFAR
	98	112	15	ASFRLFARTSMWSF
	116	130	15	TNILLNVPLHGTILT
	144	158	15	ILRGHLRIAGHHLGR
	165	179	15	PKEITVATSRTLSYY
	175	189	15	TLSYKLGASQRVAG
Nucleoprotein	107	121	15	RWYFYLLGTGPEAGL
	129	143	15	GIIVVATEGALNTPK
	154	168	15	NAAIVLQLPQGTTL
	303	317	15	QIAQFAPSASAFFGM
	328	342	15	GTWLTYTGAIKLDDK
	387	401	15	KKQQTVTLLPAADLD

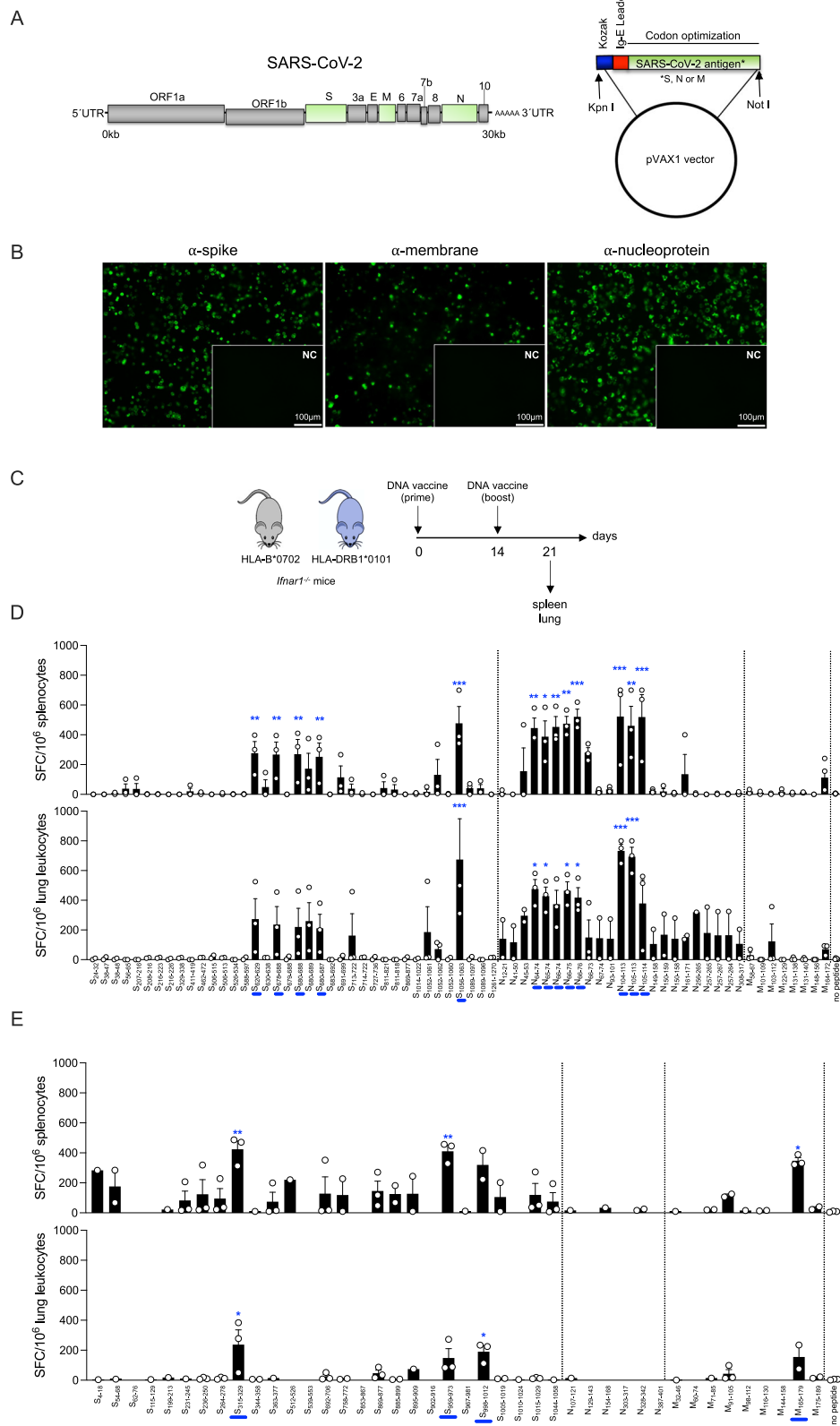
investigate whether exposure to seasonal common cold HCoVs can elicit CD8⁺ T cells that cross-react with SARS-CoV-2, we infected HLA-B*0702 *Ifnar1*^{-/-} mice with OC43, the most common seasonal HCoV worldwide^{87,88}. We then analyzed viral load in upper and lower airway tissues on days 1, 3, and 5 post-infection (Fig. S3A), and CD8⁺ T cell responses to SARS-CoV-2 peptides on days 1, 3, 5, 8, 16, and 30 post-infection (Fig. 3A). While OC43 genomic RNA levels in nasal turbinates increased between days 1 and 5, levels in lung were highest on day 1 and below the level of detection by day 5 (Figure S3B). Splenocytes prepared on days 8 and 16 post-infection with OC43 were stimulated with a panel of 37 HLA-B*0702-restricted SARS-CoV-2 CD8⁺ T cell epitopes previously shown to stimulate human CD8⁺ T cells based on IFN γ -

ELISpot or ICS assays (NIAID Virus Pathogen Database and Analysis Resource; Table 3)^{25,89–95}. These 37 peptides from SARS-CoV-2 M ($n = 3$), N ($n = 7$), ORF1ab ($n = 24$), ORF7 ($n = 2$), and ORF8 ($n = 1$) proteins—were selected to ensure that the analysis of OC43-elicited T cell reactivity was focused on the most human-relevant SARS-CoV-2 epitopes. The only significant activated CD8⁺ T response was at day 16 post-OC43 infection, and was focused on a single region in the N protein, with 9- and 12-fold expansion of N₁₀₄₋₁₂₁-reactive IFN γ ⁺ and IFN γ /TNF⁺ CD8⁺ T cells, respectively (Fig. 3B, with the gating strategy represented in Fig. S2C). To validate this finding, splenocytes and lung leukocytes isolated on day 8 post-infection were stimulated with the 69-peptide panel (Table 1 and Fig. 1C). Indeed, the frequencies of IFN γ -producing splenocytes and lung leukocytes were increased by only 3 SARS-CoV-2 peptides, all encompassing the N₁₀₄₋₁₁₃ epitope (Fig. 3C). Thus, exposure to OC43 elicits HLA-B*0702-restricted CD8⁺ T cells with reactivity to the SARS-CoV-2 N₁₀₄₋₁₁₃ epitope. Of note, the SARS-CoV-2 and OC43 N₁₀₄₋₁₁₃ sequences differ by a single amino acid residue (LSPRWYFYLL and LLPRWYFYLL, respectively), providing a basis for this cross-reactivity.

We extended this investigation by following the development of the SARS-CoV-2 N₁₀₄₋₁₁₃-reactive effector CD8⁺ T cell response in the spleen and lung for a period of 30 days following OC43 infection (Fig. 3A, D). The gating strategy is represented in Fig. S2A. Expansion of N₁₀₄₋₁₁₃-reactive IFN γ ⁺ and IFN γ /TNF⁺ CD8⁺ T cells was evident by day 8 and remained stable (IFN γ ⁺) or increased slightly (IFN γ /TNF⁺) by day 30. In contrast, polyfunctional IFN γ ⁺/TNF⁺/IL-2⁺ cells were undetectable until day 30, at which point a small but significant expansion of SARS-CoV-2 N₁₀₄₋₁₁₃-reactive cells was detected in the spleen but not the lung. Finally, IFN γ ⁺/CD107a⁺ CD8⁺ T cells exhibited a biphasic response detected in the spleen by day 8, had waned by day 16, and increased again by day 30. These data provide the first direct demonstration that the seasonal coronavirus OC43 elicits SARS-CoV-2 cross-reactive CD8⁺ T cells. They also show that this cross-reactive response is directed against a single immunodominant SARS-CoV-2 epitope, N₁₀₄₋₁₁₃, in the context of HLA-B*0702.

OC43 infection elicits CD4⁺ T cells with cross-reactivity to SARS-CoV-2

To determine whether OC43 infection can also induce a CD4⁺ T cell response that cross-reacts with SARS-CoV-2, HLA-DRB1*0101 *Ifnar1*^{-/-} mice were infected with OC43, and spleens and lungs harvested on days 8, 16, and 30 post-infection (Fig. 4A). Splenocytes and lung leukocytes isolated on day 8 were stimulated with the same 42-panel of SARS-CoV-2 peptides (Table 1) used to stimulate cells from DNA-vaccinated and SARS-CoV-2-infected mice (Figs. 1D and 2C, respectively). The frequencies of IFN γ -producing splenocytes were increased by 4 SARS-CoV-2 peptides (S₅₄₋₆₈, S₂₆₄₋₂₇₈, S₇₅₈₋₇₇₂, and M₃₂₋₄₆), and IFN γ -producing lung leukocytes were increased by 1 (S₂₆₄₋₂₇₈) (Fig. 4B). To validate the CD4⁺ T cell cross-reactivity in this model, splenocytes were stimulated with a panel of 37 HLA-DRB1*0101-restricted peptides derived from SARS-CoV-2 E, S, M, N, ORF1ab, ORF3a, and ORF8 proteins (Table 4) previously shown to stimulate human CD4⁺ T cell responses by IFN γ -ELISpot, ICS, or MHC-binding assays^{18,90,96-100} (Fig. 4C). The gating strategy is represented in Fig. S2D. At day 8, IFN γ ⁺ CD4⁺ T cells reactive with all 37 peptides were expanded in the spleen, although the increase was statistically significant only for cells stimulated with M₆₆₋₈₀ and ORF3a₁₁₆₋₁₃₀. At day 16, frequencies of IFN γ ⁺ CD4⁺ T cells cross-reactive with SARS-CoV-2 ORF8₉₆₋₁₁₀ and ORF8₁₀₁₋₁₁₅ were significantly increased. In contrast, polyfunctional SARS-CoV-2 cross-reactive IFN γ ⁺/TNF⁺ CD4⁺ T cells were significantly expanded only in response to N₈₆₋₁₀₀ and N₂₆₁₋₂₇₅ peptides. In addition, while N₈₆₋₁₀₀ and ORF3a₁₀₈₋₁₂₀ peptides stimulated IL-2 production at day 16, none of the 37 peptides stimulated IL-4 expression (Fig. S3G). Finally, at day 30, the CD4⁺ T cell response was decreased for all peptides. Thus, exposure to OC43 elicits a Th1-biased CD4⁺ T cell response that cross-reacts with



SARS-CoV-2 in the context of HLA-DRB1*0101. Viral load analysis on days 1, 3, and 5 post-infection (Fig. S3A) revealed levels of OC43 genomic RNA that were high in nasal turbinates on all 3 days and dramatically lower in lung (undetectable on day 1 and rising significantly but only slightly by day 3; Fig. S3C).

We next examined whether OC43 infection stimulates a SARS-CoV-2 cross-reactive antibody response in the context of HLA-

DRB1*0101, given that CD4⁺ T cells play crucial roles in promoting and maintaining antibody responses^{101,102}. To this end, serum was isolated from the OC43-infected mice at 6 time points from 0 to 100 days post-infection (Fig. S3D) and analyzed by ELISA for antibodies that bind to OC43 or SARS-CoV-2 S and N proteins. Anti-OC43 S IgG titers were detectable by day 14 and remained relatively stable up to day 100; in contrast, IgG reactive with SARS-CoV-2 S protein was not detected in

Fig. 1 | Mapping SARS-CoV-2 S, N, and M protein-derived epitopes in DNA-vaccinated HLA-B*0702 and HLA-DRB1*0101 *Ifnar1*^{-/-} mice. **A** SARS-CoV-2 genome and DNA vaccine constructs containing mammalian-optimized Kozak sequence, IgE leader sequence, and codon-optimized DNA sequence for SARS-CoV-2 S, N, or M protein. **B** Representative immunofluorescence images of 293 T cells transfected with S, M, or N DNA vaccines (*vs* empty vector [insets]) and immunolabeled for SARS-CoV-2 S, N, or M protein (green). Scale bars apply to main panels and insets. Images are representative of 2 independent experiments. **C** Experimental protocol for D and E. HLA-B*0702 and HLA-DRB1*0101 *Ifnar1*^{-/-} mice were administered 25 μg S, N, or M DNA vaccines by intramuscular electroporation

on days 0 and 14, and tissue collected 7 days later. **D, E** ELISpot quantification of IFN γ -producing spot-forming cells (SFC) from HLA-B*0702 *Ifnar1*^{-/-} mice (**D**) and HLA-DRB1*0101 *Ifnar1*^{-/-} mice (**E**). Splenocytes and lung leukocytes were stimulated for 20 h with 69 (**D**), or 42 (**E**) SARS-CoV-2 peptides predicted to be immunogenic for CD8⁺ T cells (**D**) or CD4⁺ T cells (**E**; Tables 1 and 2); control, no peptide. Data are presented as the mean \pm SEM; *N* = 4 mice/group pooled from 2 independent experiments. Peptide *vs* control were compared using the one-way ANOVA test. The mean of each peptide was compared to the mean of the control (no peptide). **P* < 0.05; ***P* < 0.01; ****P* < 0.001. Blue bars on the *x*-axis are peptides that significantly stimulated 1 or more cell types.

sera of OC43-infected mice at any time point (Fig. S3E). IgG titers against the N proteins of both OC43 and SARS-CoV-2 were minimal at all time points (Fig. S3F). Thus, in our model of primary OC43 infection in HLA-DRB1*0101 *Ifnar1*^{-/-} mice, OC43 S-specific IgG and SARS-CoV-2-reactive CD4⁺ T cells are present. These data demonstrate that prior exposure to OC43 elicits an HLA-DRB1*0101-restricted CD4⁺ T cell response that cross-reacts with SARS-CoV-2 epitopes.

Immunization with N₁₀₄₋₁₁₃ peptide protects against SARS-CoV-2 infection and lung damage in HLA-B*0702 *Ifnar1*^{-/-} mice

To determine whether the OC43 cross-reactive CD8⁺ T cell response can protect against or exacerbate SARS-CoV-2 infection and/or pathology, HLA-B*0702 *Ifnar1*^{-/-} mice were primed and boosted with N₁₀₄₋₁₁₃ peptide on days 0 and 21, challenged with SARS-CoV-2 B.1.351 at 14 days post-boost, and tissues harvested 3 days later (Fig. 5A, with the gating strategy represented in Fig. S2E). In splenocytes from N₁₀₄₋₁₁₃-immunized mice (*vs* mock-immunized), the frequencies of N₁₀₄₋₁₁₃-reactive IFN γ ⁺, polyfunctional (IFN γ ⁺/TNF⁺ and IFN γ ⁺/TNF⁺/IL-2⁺) and cytotoxic multifunctional (IFN γ ⁺/CD107a⁺) CD8⁺ T cells were significantly increased (Fig. 5B), and lung appeared healthier by histopathology (Fig. 5C). In fact, quantification of histopathology data revealed 3 features of SARS-CoV-2-induced lung disease that were less pronounced (lower scores) in N₁₀₄₋₁₁₃-immunized mice, although these differences were not significant: necrosis of bronchiolar epithelial cells (BEC), cellular debris in bronchioles, and suppurative bronchiolitis. When the Fig. 5A experiment was repeated with the MA10 strain of SARS-CoV-2 (Fig. S4A), our findings were confirmed: the N₁₀₄₋₁₁₃-immunized mice had significantly higher frequencies of N₁₀₄₋₁₁₃-reactive polyfunctional CD8⁺ T cells (Fig. S4B) and significantly lower histopathology scores (Fig. S4C). For the B.1.351-challenged mice, we also analyzed viral burden. Both RT-qPCR analysis of genomic RNA (Fig. 5D) and immunofluorescence analysis of SARS-CoV-2 N protein (Fig. 5E) revealed significantly lower levels of SARS-CoV-2 in lungs of N₁₀₄₋₁₁₃-immunized mice. These results demonstrate that immunization of HLA-B*0702 *Ifnar1*^{-/-} mice with SARS-CoV-2 N₁₀₄₋₁₁₃ peptide elicits an antigen-specific polyfunctional CD8⁺ T cell response and protects against SARS-CoV-2 infection and lung disease.

Prior exposure to OC43 confers cross-protection against SARS-CoV-2 infection in HLA-B*0702 *Ifnar1*^{-/-} mice

Given that N₁₀₄₋₁₁₃-immunization reduced SARS-CoV-2 burden and pathogenesis, we hypothesized that OC43-elicited CD8⁺ T cell immunity might be similarly protective. To test this, HLA-B*0702 *Ifnar1*^{-/-} mice were infected with OC43 and challenged with SARS-CoV-2 on day 8 or 16 post-infection (Fig. S5A) or 60–70 days post-infection (Fig. 5F). Immunologic and virologic phenotypes were analyzed at 3 days post-challenge, which allowed us to focus on the effects of OC43-elicited immunity—rather than the primary T cell response to the SARS-CoV-2 challenge (primary antiviral T cell responses are generally not detectable until days 4 or 5 post-infection^{47,48,74}).

To test for the presence of the OC43-elicited cross-reactive CD8⁺ T cell response in HLA-B*0702 *Ifnar1*^{-/-} mice, splenocytes from OC43-exposed (*vs* naïve) SARS-CoV-2-challenged mice were stimulated with N₁₀₄₋₁₁₃ peptide and analyzed by ICS (Fig. 5G). Polyfunctional CD8⁺

T cells were significantly increased in mice challenged at 60–70 days post-OC43 infection (Fig. 5G). In contrast, in mice challenged at 8 or 16 days, activated effector CD8⁺ T cell subsets expanded, but these increases were generally insignificant (Fig. S5B). RT-qPCR analysis revealed no effect of OC43 pre-exposure on SARS-CoV-2 genomic RNA levels in either lungs or nasal turbinates of mice challenged on days 8 or 16 (Fig. S5C). In contrast, lungs from mice challenged 60 to 70 days post-OC43 infection exhibited dramatic reductions in both SARS-CoV-2 genomic RNA (Fig. 5H) and N-protein immunoreactivity (Fig. 5I). While blinded histopathological analysis of lungs revealed no differences between OC43-infected and naïve mice challenged at 8 or 16 days post-infection (Fig. S5D), OC43-infected mice challenged at 60 to 70 days tended to have more bronchioles with clear lumina and viable epithelial cells lining the airway (i.e., proper polarization), and exhibited decreases in 3 histopathologic features (necrotic epithelial cells, cellular debris within bronchioles, and bronchiolar lesions), which were, however, not significant (Fig. 5J). Thus, a single prior intranasal exposure to OC43 can protect against SARS-CoV-2 infection in HLA-B*0702 *Ifnar1*^{-/-} mice and may also limit SARS-CoV-2-induced lung damage in some mice. The immunologic and virologic data together suggest that OC43-elicited SARS-CoV-2-cross-reactive CD8⁺ T cells may contribute to the cross-protection against SARS-CoV-2 infection.

OC43 infection confers cross-protection against SARS-CoV-2 in HLA-DRB1*0101 *Ifnar1*^{-/-} mice in a manner partially dependent on CD4⁺ T cells

We have shown that HLA-DRB1*0101 *Ifnar1*^{-/-} mice, mount an antigen-specific CD4⁺ T cell response against SARS-CoV-2 after DNA vaccination or viral infection (Figs. 1E and 2C), and a CD4⁺ T cell response to OC43 that cross-reacts with SARS-CoV-2 (Figs. 4 and S3G). To determine whether OC43 pre-exposure can protect against SARS-CoV-2, HLA-DRB1*0101 *Ifnar1*^{-/-} mice were infected with OC43, challenged with SARS-CoV-2 16 days later (SARS-CoV-2 cross-reactive Th1 CD4⁺ T cell response peaked at 16 days post-OC43 infection; Fig. 4C), and lungs were harvested at 3 days post-challenge (Fig. 6A). Prior OC43 exposure led to dramatically lower levels of SARS-CoV-2 infection in the lungs, based on RT-qPCR analysis of SARS-CoV-2 genomic RNA and immunostaining for N protein (Fig. 6B, C), but did not significantly affect SARS-CoV-2 RNA levels in nasal turbinates (Fig. S6A). Histopathological analysis showed that the lungs of OC43-exposed/SARS-CoV-2-challenged mice were much healthier than those of naïve/SARS-CoV-2-challenged mice. Specifically, OC43 pre-exposure led to more bronchioles with clear lumina, viable epithelial cells, and significant improvement in all 5 features (Fig. 6D). Thus, OC43 pre-exposure for 16 days was sufficient to elicit a cross-protective response against SARS-CoV-2 infection and lung disease in HLA-DRB1*0101 *Ifnar1*^{-/-} mice.

The majority of SARS-CoV-2-specific T cell responses in humans are CD4⁺ T cells^{31,103,104}. To determine whether the protective effects of OC43 pre-exposure were mediated by CD4⁺ T cells, we repeated these experiments in mice treated with a CD4 T cell-depleting antibody (*vs* isotype) immediately prior to SARS-CoV-2 challenge (Fig. 6E). Efficient CD4⁺ T cell depletion, confirmed by flow cytometry (Figure S6C),

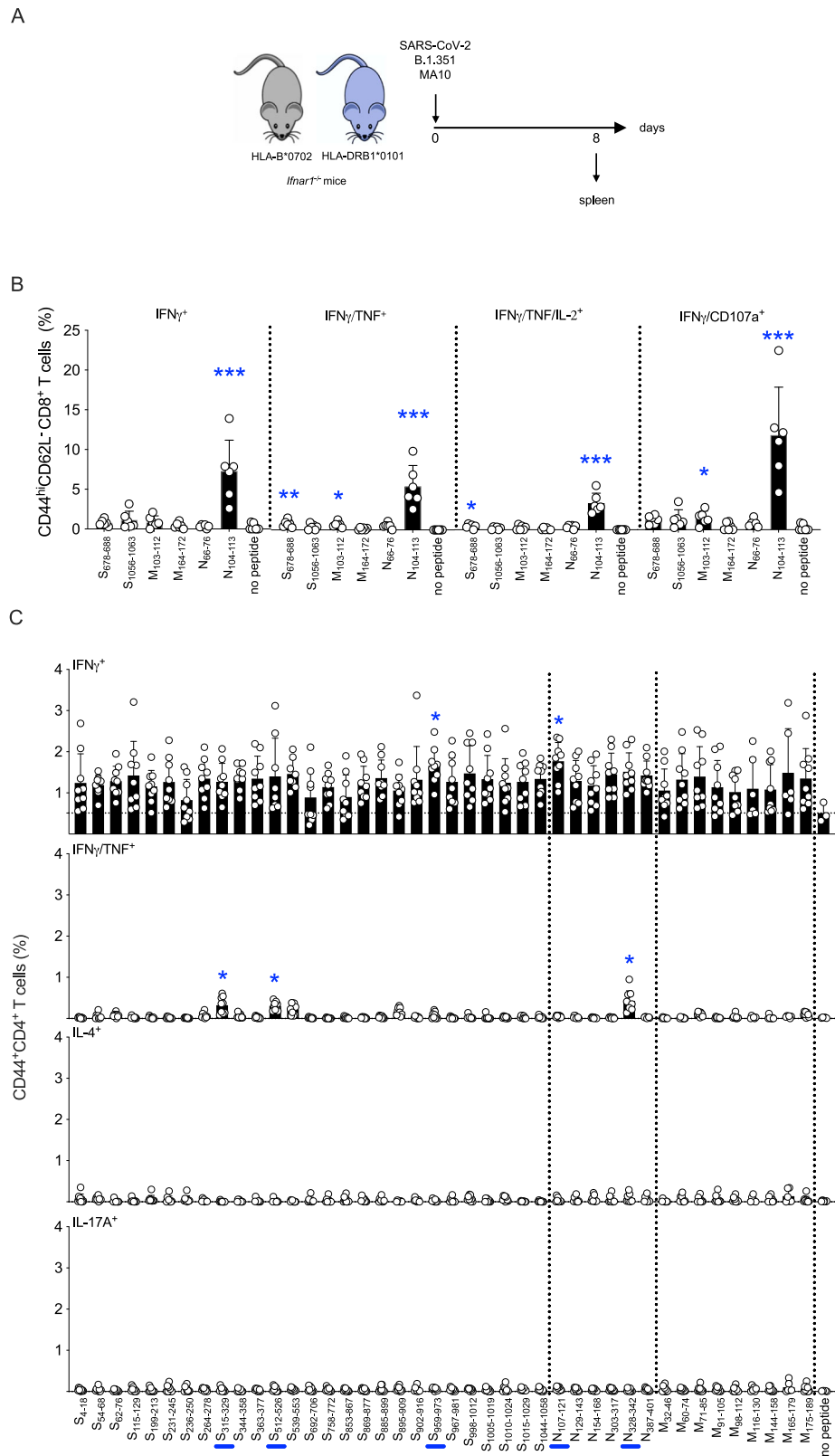
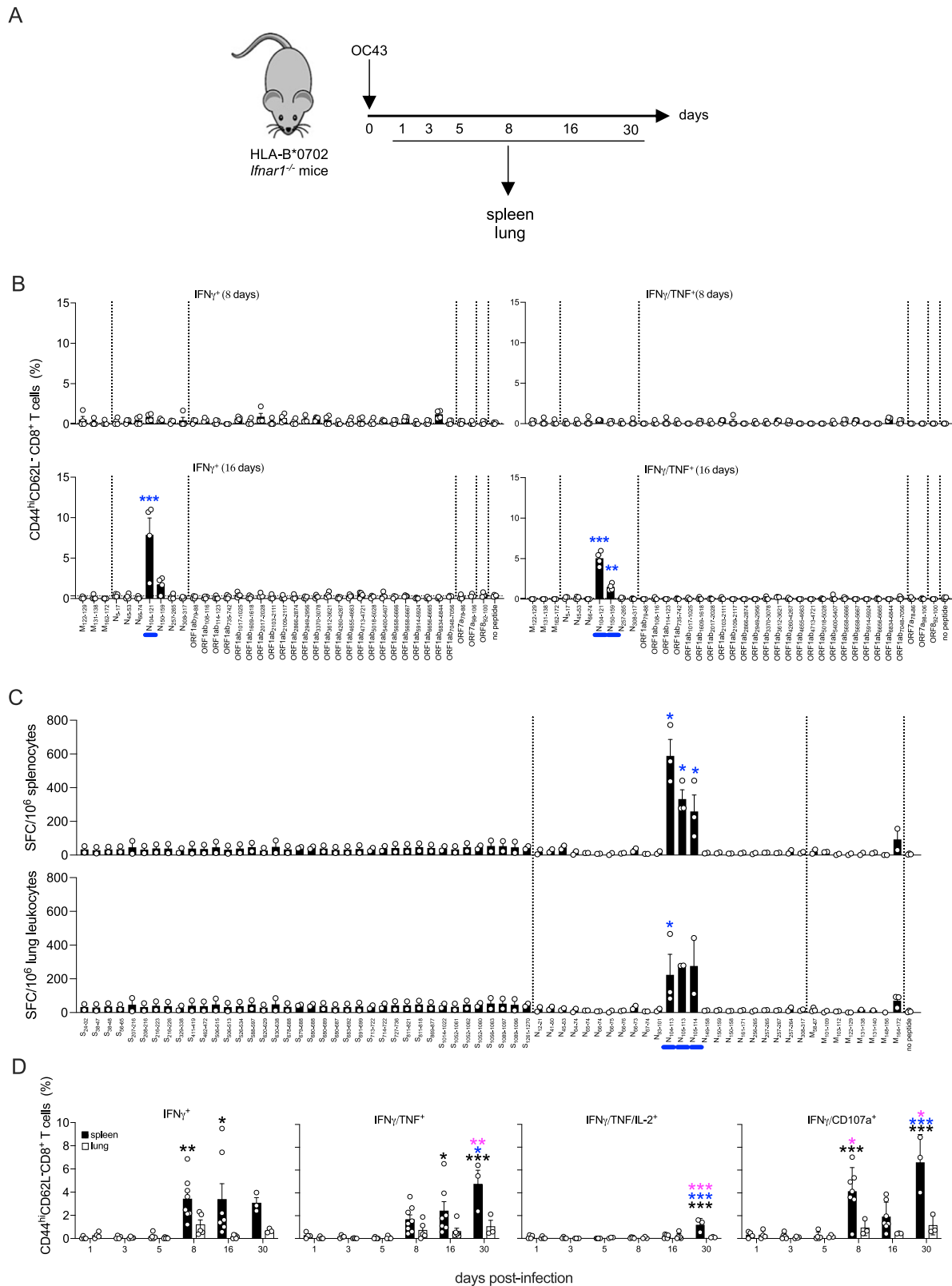


Fig. 2 | Mapping of SARS-CoV-2 S, N, and M protein-derived epitopes in SARS-CoV-2-infected HLA-B*0702 and HLA-DRB1*0101 *Ifnar1*^{-/-} mice. **A** Experimental protocol. HLA-B*0702 and HLA-DRB1*0101 *Ifnar1*^{-/-} mice were infected with SARS-CoV-2 strains B.1.351 or MA10, respectively (10⁴ PFU, IN), and spleens collected 8 days later. **B**, **C** ICS analysis of activated CD8⁺ T cells from B.1.351-infected HLA-B*0702 *Ifnar1*^{-/-} mice (**B**) and activated CD4⁺ T cells from MA10-infected HLA-DRB1*0101 *Ifnar1*^{-/-} mice (**C**). Splenocytes were stimulated for 6 h with the indicated

6 (**B**) or 42 (**C**) SARS-CoV-2 peptides (*vs* no peptide), immunolabeled for cell surface markers, intracellular cytokines, and the degranulation marker CD107a, and analyzed by flow cytometry. Data are presented as the mean ± SEM. N values: 6 (**B**) and 9 (**C**) mice/group, pooled from 2 independent experiments. Peptide *vs* control were compared using the nonparametric Kruskal–Wallis test. **P* < 0.05; ***P* < 0.01; ****P* < 0.001. Circles, individual mice. Blue bars on the x-axis, peptides that significantly stimulated CD4⁺ T cells with at least 1 secretion phenotype.



significantly reduced the protective effect of prior OC43 exposure on SARS-CoV-2 genomic RNA levels and N protein expression in lungs (Fig. 6F, G). However, CD4⁺ T cell-depleted, and isotype control mice (both OC43 infected) showed indistinguishable features of mild pneumonia in the lungs (Fig. 6H) and no difference in SARS-CoV-2 genomic RNA levels in nasal turbinates (Figure S6B). This indicates that OC43-elicited CD4⁺ T cells contribute to cross-protection against

SARS-CoV-2 infection but do not significantly affect lung disease at day 3 after infection.

Discussion

The emergence of novel SARS-CoV-2 variants, increasingly prevalent infections and breakthrough infections have highlighted the relatively narrow immune response elicited by the currently available SARS-CoV-

Fig. 3 | Cross-reactivity of OC43-elicited CD8⁺ T cells for SARS-CoV-2 peptides. **A** Experimental protocol. HLA-B*0702 *Irfar1*^{-/-} mice were infected with OC43 (10⁹ genomic equivalents (GE), IN), and tissues were collected on multiple days. **B** ICS analysis of activated CD8⁺ T cells in splenocytes stimulated for 6 h with 1 of 37 published HLA-B*0702-restricted SARS-CoV-2-derived peptides (Table 2) *vs* no peptide, immunolabeled for cell surface markers and intracellular cytokines, and analyzed by flow cytometry. Circles, individual mice; *N* = 4 mice/group. **C** ELISpot quantification of IFN γ -producing SFCs in splenocytes and lung leukocytes isolated on day 8 post-infection and stimulated for 20 h with 69 SARS-CoV-2 peptides (Table 1) *vs* no peptide. *N* = 6 mice/group. **D** ICS analysis of activated CD8⁺ T cells in splenocytes (black bars) and lung leukocytes (white bars) isolated on multiple days.

Cells were stimulated for 6 h with SARS-CoV-2 N₁₀₄₋₁₁₃ peptide, immunolabeled for cell surface markers, intracellular cytokines, and CD107a, and analyzed by flow cytometry. Circles, individual mice; *N* = 4, 4, 5, 8, 7, and 3 mice/group for spleen samples and *N* = 4, 4, 5, 5, 6, and 3 for lung leukocytes samples from days 1, 3, 5, 8, 16, and 30, respectively. Black, blue, and pink asterisks, comparisons *vs* day 1, day 8, and day 16 data, respectively. **B–D** Data, pooled from two independent experiments, are presented as the mean \pm SEM, and compared by either the nonparametric Kruskal–Wallis test (**B, C**) or two-way ANOVA with Sidak's multiple comparison test (**D**). **P* < 0.05; ***P* < 0.01; ****P* < 0.001. Blue bars on the x-axis in **B** and **C**, peptides that significantly stimulated 1 or more cell groups.

2 vaccines. A substantial fraction of these breakthrough infections occurred in immunocompromised people, in which viral evolution may lead to the generation of new VOCs¹⁰⁵. In contrast to the anti-SARS-CoV-2 antibody response, which is focused on the highly variable S protein, T cells contribute to protection against SARS-CoV-2 by

recognizing conserved epitopes of multiple SARS-CoV-2 proteins^{106–110}, particularly in the context of impaired humoral immunity^{111–116}. In addition, T cells that recognize homologous epitopes between seasonal HCoVs and SARS-CoV-2 are present in some healthy individuals previously unexposed to SARS-CoV-2^{18,21,23,29,82,93,117,118}. Importantly, robust pre-existing HCoV/SARS-CoV-2 cross-reactive T cell responses that are rapidly induced following SARS-CoV-2 exposure have been associated with asymptomatic infection and less severe COVID-19, suggesting a role for these cells in protective immunity to SARS-CoV-2^{23,29,39,41,81,119}. Therefore, understanding the pre-existing SARS-CoV-2 cross-reactive T cell responses in SARS-CoV-2 naïve individuals helps explain the broad heterogeneity in COVID-19 outcomes and to develop pan-CoV vaccines that could provide broad protection against current and future SARS-CoV-2 variants and HCoVs.

Table 3 | HLA-B*0702-restricted CD8⁺ T cell epitopes identified in the literature (May 2021)

Protein	Start	End	Length	Sequence
Membrane	122	129	8	VPLHGTL
	131	138	8	RPLLESEL
	164	172	9	LPKEITVAT
Nucleocapsid	5	17	13	GPQNQRNAPRITF
	45	53	9	LPNNTASWF
	66	74	9	FPRGQGVPI
	104	121	18	LSPRWYFYLLGTGPEAGL
	150	159	10	NPANNAIVL
	257	265	9	KPRQKRTAT
	308	317	10	APSASAFFGM
ORF1ab	79	88	10	APHGHVMVEL
	108	116	9	VPHVGEIPV
	114	123	10	IPVAYRKVLL
	735	742	8	APKEIFL
	1017	1025	9	TPVVQTIEV
	1608	1618	11	KPHNSHEGKTF
	2017	2028	12	KPVETSNSFDVL
	2109	2117	9	KPNELSRVL
	2703	2711	9	VAKSHNIAL
	2866	2874	9	VGPLPGTIL
	2949	2956	8	RPDTRYVL
	3370	3378	9	QPGQTFSVL
	3612	3621	10	LPFAMGIAM
	4260	4267	8	VPANSTVL
	4655	4663	9	KPYIKWDLL
	4713	4721	9	FPPTSFGPL
	5018	5028	11	MPNMLRIMASL
	5400	5407	8	KPPISFPL
	5658	5666	9	IPARARVEC
	5658	5667	10	IPARARVECF
5914	5924	11	LEIPRRNVATL	
6656	6665	10	KPRSQMEIDF	
6834	6844	11	LPKGIMMNV	
7048	7056	9	FPLKLRGTA	
ORF7	78	86	9	RARSVSPKL
	98	106	9	SPIFLIVAA
ORF8	92	100	9	EPKLGSLVV

Multiple human studies suggest that pre-existing SARS-CoV-2 cross-reactive T cells derive, partly or wholly, from exposure to seasonal HCoVs^{39,120,121} and can have either protective or pathogenic consequences for subsequent SARS-CoV-2 infection. To test this directly, we used HLA-B*0702 and HLA-DRB1*0101 transgenic *Irfar1*^{-/-} mice. We found that primary SARS-CoV-2 infection or vaccination with SARS-CoV-2 protein-encoding vectors elicited CD8⁺ and CD4⁺ T cell responses that recapitulated the epitope specificity, Tc1- and Th1-bias, and monofunctional/multifunctional phenotypes observed in SARS-CoV-2-infected or vaccinated humans^{18,21,23,29,82,93,117,122}. OC43-SARS-CoV-2 sequential infection of our mice showed that OC43 pre-exposure was protective against SARS-CoV-2, and this protection was partly dependent on OC43-elicited CD4⁺ T cells. It is plausible that additional elements of the pre-existing OC43 immunity, such as CD8⁺ T cells, may also contribute to this protective response. Our findings present direct experimental evidence for a protective role for seasonal HCoV/SARS-CoV-2 cross-reactive CD4⁺ T cell responses, consistent with human data implicating cross-reactive CD4⁺ T cells in protecting against SARS-CoV-2 infection^{23,29,39,40,42,119,123,124}. They also align with a mouse study demonstrating that CD4⁺ T cells recognizing a conserved epitope present in SARS-CoV, MERS-CoV, and bat CoV HKU4 are cross-protective¹²⁵. We detected minimal cross-reactive humoral response to SARS-CoV-2 in HLA-DRB1*0101 transgenic *Irfar1*^{-/-} mice pre-exposed to OC43, which is consistent with data showing no significant cross-reactivity of human anti-HCoV antibodies with SARS-CoV-2^{126,127}, and broadly coronavirus-reactive antibodies in very few SARS-CoV-2-immune individuals^{128–131}. In fact, human studies have reported that the weak, cross-reactive antibody response decays rapidly in most individuals, and the cross-reactive cellular but not humoral immunity likely contributes to significant protection against SARS-CoV-2^{18,132–135}. In line with the report that the CD4⁺ T cell cross-reactivity to SARS-CoV-2 in healthy SARS-CoV-2-unexposed individuals is variable and low, and that the degree of amino acid sequence identity between common cold HCoVs and SARS-CoV-2 does not correlate with CD4⁺ T cell cross-reactivity³⁶, some of the OC43-elicited SARS-CoV-2 cross-reactive CD4⁺ T cell specificities in our mouse model are of low magnitude and share limited amino acid sequence homology between OC43 and SARS-CoV-2.

The level of protection mediated by pre-existing, cross-reactive T cells may be influenced by modulation of immunodominance

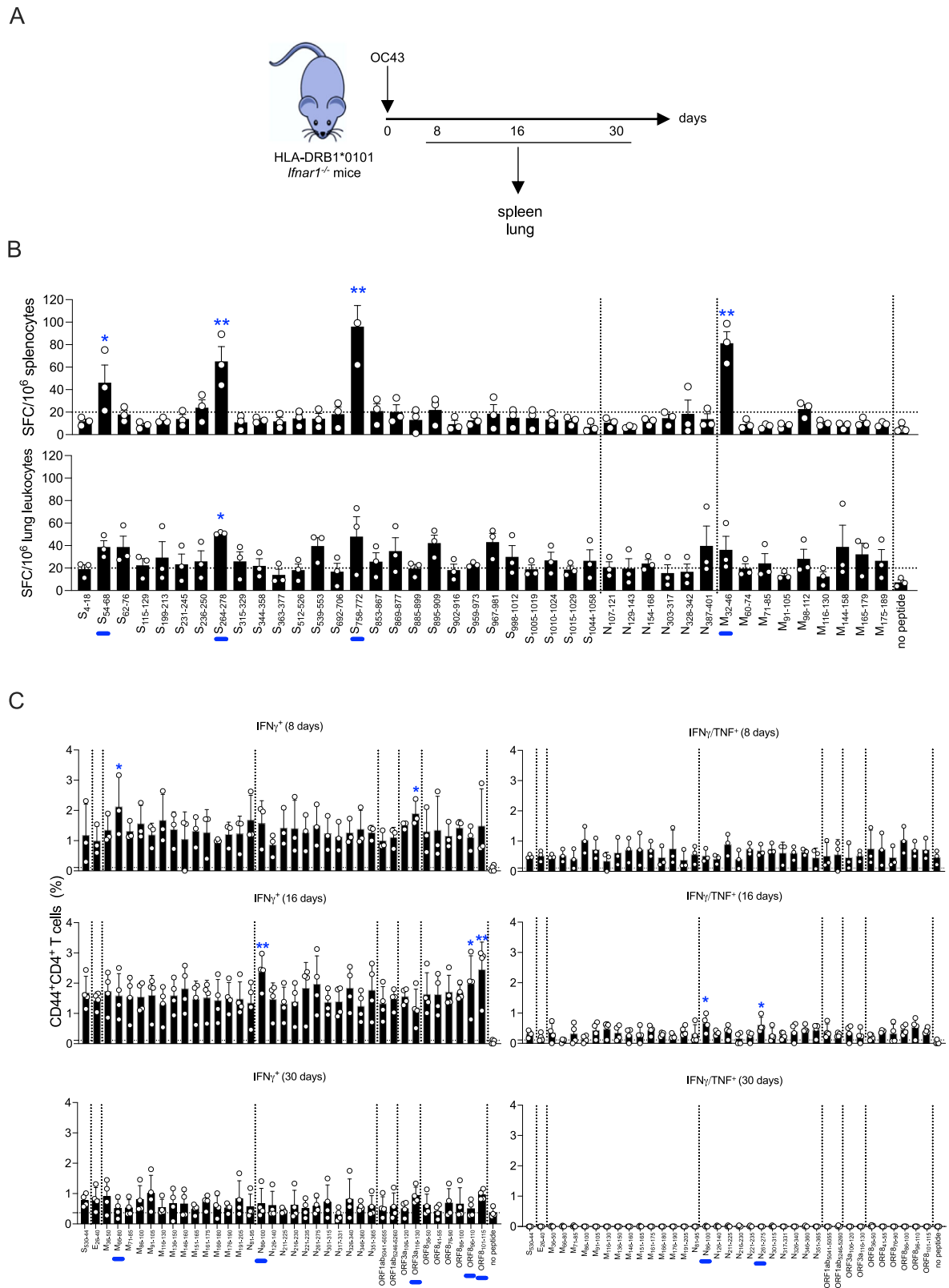


Fig. 4 | Cross-reactivity of OC43-elicited CD4⁺ T cells for SARS-CoV-2 peptides. **A** Experimental protocol. HLA-DRB1*0101 *Ifnar1*^{-/-} mice were infected with OC43 (10⁹ GE, IN), and tissues were collected 8, 16, and 30 days later. **B** ELISpot quantification of IFN γ -producing SFCs in splenocytes and lung leukocytes isolated on day 8 post-infection and stimulated for 20 h with 42 SARS-CoV-2 peptides (Table 2) *vs* no peptide. *N* = 8 mice/group. **C** ICS analysis of activated CD4⁺ T cells in splenocytes isolated on days 8, 16, and 30 post-infection. Cells were stimulated for 6 h with the 37 published HLA-DRB1*0101-restricted SARS-CoV-2-derived peptides (Table 4) *vs* no peptide, immunolabeled for cell surface markers and intracellular cytokines, and analyzed by flow cytometry. Circles, individual mice; *N* = 4 mice/group. **B, C** Data, pooled from two independent experiments and presented as the mean \pm SEM, were compared by the nonparametric Kruskal–Wallis test. **P* < 0.05; ***P* < 0.01. Blue bars on the x-axis are peptides that significantly stimulated 1 or more cell groups.

Table 4 | HLA-DRB1*0101-restricted CD4⁺ T cell epitopes identified in the literature (May 2021)

Protein	Start	End	Length	Sequence
Spike	530	544	15	STDLIKNQCVNFNFN
Envelope	26	40	15	FLVLTALAILTALRLC
Membrane	36	50	15	QFAYANRRNRFYIIK
	66	80	15	VLAAYRINWITGGI
	71	85	15	YRINWITGGIAIAMA
	86	100	15	CLVGLMWLSYFIASF
	91	105	15	MWLSYFIASFRLFAR
	116	130	15	TNILLNVLHGILT
	136	150	15	SELVIGAVILRGHLR
	146	160	15	RGHLRIAGHHLGRCD
	151	165	15	IAGHHLGRCDIKDLP
	161	175	15	IKDLPKEIVATSRT
	166	180	15	KEIVATSRTLSYYK
	176	190	15	LSYYKLGASQRVAGD
191	205	15	SGFAAYSRYRIGNYK	
Nucleoprotein	81	95	15	DDQIGYRRATRRIR
	86	100	15	YYRRATRRIRGGDGK
	126	140	15	NKDGIWVATEGALN
	211	225	15	AGNGGDAALALLLLD
	216	230	15	DAALALLLLDRLNQL
	221	235	15	LLLLDRLNQLSKMS
	261	275	15	KRTATKAYNVTQAFG
	301	315	15	WPQIAQFAPSASAFF
	317	331	15	MSRIGMEVTPSGTWL
	326	340	15	PSGTWLTGTGAIKLD
346	360	15	FKDQVILLNKHIDAY	
351	365	15	ILLNKHIDAYKTFPP	
ORF1ab	5041	5055	15	SHRFYRLANECAQVL
	5246	5260	15	LMIERFVSLAIDAYP
ORF3a	106	120	15	LYLYALVYFLQSINF
	116	130	15	QSINFVRIIMRLWLC
ORF8	36	50	15	PCPIHFYSKYIIRVG
	41	55	15	FYSKYIIRVGARKSA
	76	90	15	IGNYTVSCLPFTINC
	86	100	15	FTINCQEPKLGSLVV
	96	110	15	GSLVVRCSFYEDFLE
101	115	15	RCSFYEDFLEYHDVR	

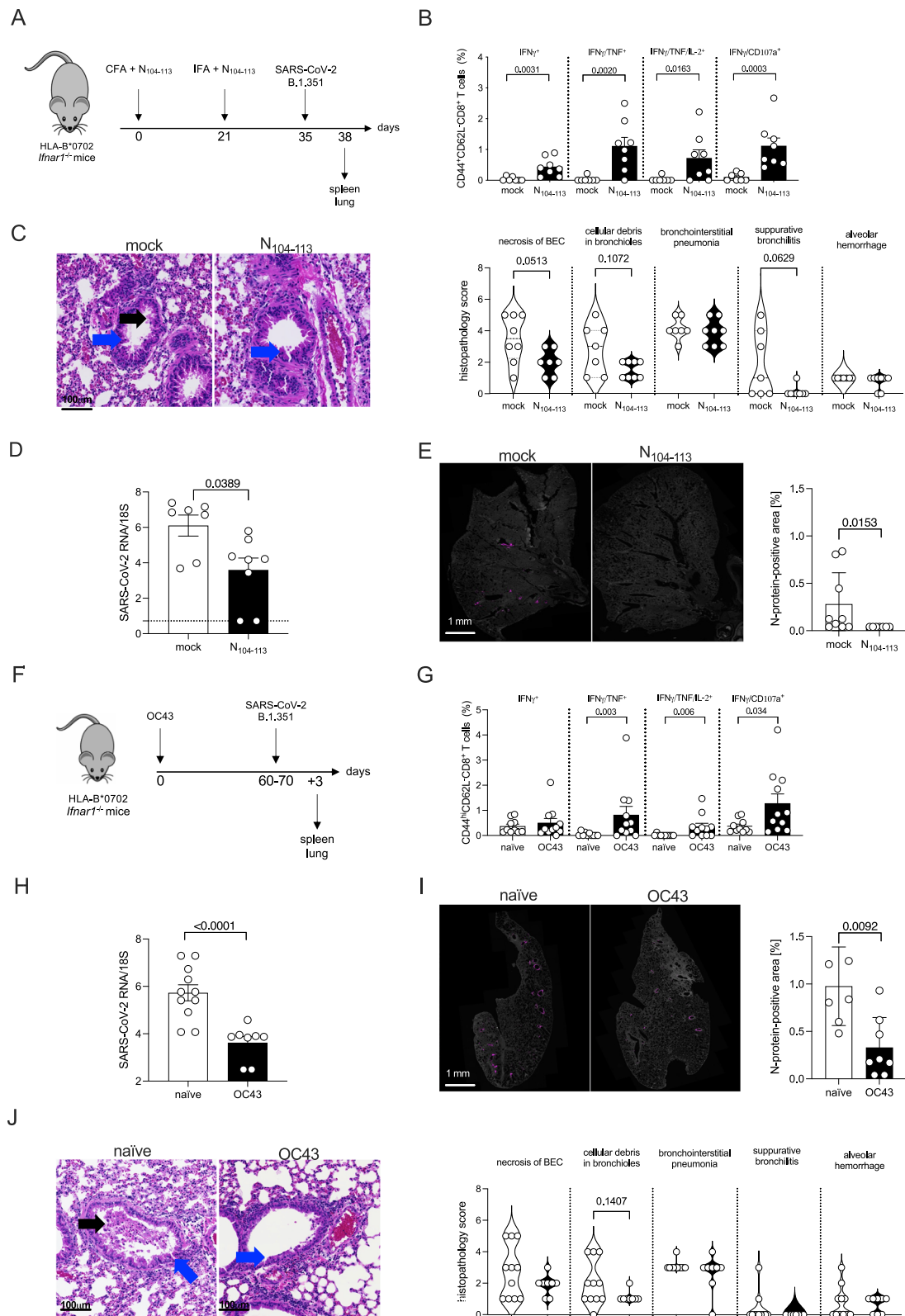
hierarchies, as observed during Zika virus infection in humans and HLA transgenic mice with prior exposure to dengue virus^{74,136}. Accumulating evidence suggests that immunodominance may be an important feature of the T cell response to SARS-CoV-2. For example, in a single cohort of SARS-CoV-2-infected individuals, researchers identified 2 populations of SARS-CoV-2 S protein-specific CD4⁺ T cells that were differentially activated: S₇₅₁- and S₂₃₆-specific, which were dominant and subdominant, respectively¹³⁷. In addition, T cells recognizing an immunodominant seasonal HCoV/SARS-CoV-2 cross-reactive epitope restricted by HLA-B*1501 are observed in SARS-CoV-2 naïve and exposed individuals³⁹. Similarly, CD8⁺ T cells recognizing the HLA-B*0702-restricted SARS-CoV-2 epitope N₁₀₅₋₁₁₃ (the most immunodominant SARS-CoV-2 CD8⁺ T cell epitope identified to date) are present at high frequencies in unexposed healthy individuals^{25,28,79-82}. Consistent with these human data, we found that CD8⁺ T cells specific for or cross-reactive with SARS-CoV-2 N_{104/105-113} epitope were immunodominant. Importantly, we observed that immunization of naïve HLA-B*0702 transgenic *Ifnar1*^{-/-} mice with the single SARS-CoV-2 N₁₀₄₋₁₁₃

peptide evoked a response that limited SARS-CoV-2-induced pathogenesis in the lung. Thus, the presence of immunodominant T cells within pre-existing SARS-CoV-2 cross-reactive T cell immunity could help to explain the disparate outcomes of COVID-19 patients.

A study in humans showed that HLA genotype shapes SARS-CoV-2-specific and memory cross-reactive CD8⁺ T cell responses¹³⁸, and another recent study reported that HLA-B*1501 associates with asymptomatic SARS-CoV-2 infection in humans³⁹. Our findings in mice expressing a single HLA allele provide a validated tool for investigating how allelic variation in HLA and infection parameters (i.e., viral strains, number and sequence of infections, and the interval between infections) influence cross-reactive T cell responses during sequential infections with seasonal HCoV and SARS-CoV-2. Our data show that a single pre-exposure to OC43 can confer cross-protection against SARS-CoV-2. However, depending on the HLA alleles and infection parameters, pre-existing HCoV-elicited T-cell immunity may also play a pathogenic role. This is supported by studies suggesting that cross-reactive CD8⁺ T cells (vs SARS-CoV-2-specific) have lower affinity⁹¹, and low-avidity SARS-CoV-2 cross-reactive CD4⁺ T cells have a reduced ability to proliferate in response to SARS-CoV-2 and are associated with more severe COVID-19^{19,38}. The present study sets a framework for investigating the role of HCoV-cross-reactive T cell responses using various HLA-expressing mice, HCoVs, and infection parameters, including sequential infections with SARS-CoV-2 followed by OC43.

In summary, the current study demonstrates a protective role for pre-existing seasonal HCoV/SARS-CoV-2-cross-reactive CD4⁺ T cell responses during SARS-CoV-2 infection. As human studies suggest both a protective and pathogenic role for HCoV-cross-reactive CD4⁺ T cell responses, a greater understanding of these T cell responses is required to facilitate T cell epitope-based rational vaccine design¹³⁹. SARS-CoV-2 vaccines that are effective in individuals with antibody or B cell deficiencies are urgently needed to protect this highly vulnerable population and limit the emergence of new VOCs. Similarly, pan-HCoV vaccines that elicit cross-protective T cell responses represent key tools against new SARS-CoV-2 VOCs and HCoVs with pandemic potential.

Limitations. Our study has several limitations. First, our findings are based on two HLA transgenic mouse strains that express a single HLA class I or II molecule, but not both, and lack a human TCR repertoire. Therefore, our results may not reflect the full spectrum of human T-cell responses. Second, OC43 RNA was detected only transiently in the lungs following infection of our two mouse strains; therefore, our observations reflect the immune response following spatially and temporally restricted exposure to OC43 antigens. Third, along similar lines, we examined the animals at 3 days post-infection in order to observe the cross-reactive memory response; however, this time point may have been suboptimal for assessing changes in lung pathology. Fourth, although type I IFN receptor deficiency has been observed in nearly 20% of severe COVID patients¹⁴⁰, anti-OC43, and anti-SARS-CoV-2 T cell responses may differ quantitatively and/or qualitatively in wildtype vs *Ifnar1*^{-/-} mice. Finally, we focused our study solely on OC43 seasonal HCoV infection prior to SARS-CoV-2 challenge, which does not model epidemiologic scenarios in which human adults are exposed to multiple seasonal HCoVs prior to SARS-CoV-2 infection. Despite these limitations, a major strength of our study is the use of mouse models in which infection parameters can be precisely controlled. Our study establishes a foundation for conducting studies using mouse models of sequential infections with NL63, 229E, or HKU1 followed by SARS-CoV-2 and investigating specific conditions and mechanisms by which HCoV-cross-reactive T cell responses contribute to protective or pathogenic immunity. Next-generation mice that co-express HLA molecules and human T cell antigen receptors¹⁴¹ are poised to further advance our understanding of the factors that dictate the heterogeneity of COVID-19 clinical and immunological outcomes.



Methods

Study design

Numerous human cohort studies have revealed that SARS-CoV-2-unexposed individuals harbor CD8⁺ and CD4⁺ T cells that recognize peptides present in both SARS-CoV-2 and seasonal HCoV. These pre-existing cross-reactive T cells have been associated with both protective

and pathologic immunity during SARS-CoV-2 infection, suggesting that they may play an important role in dictating infection outcome, which can range from asymptomatic or mild symptoms to severe COVID-19 and death. The objective of this study was to dissect the origin of pre-existing T cells that cross-react with SARS-CoV-2 and their roles during SARS-CoV-2 infection, in terms of viral load and disease outcomes.

Fig. 5 | Protective effect of OC43 pre-exposure and SARS-CoV-2 N₁₀₄₋₁₁₃ immunization on SARS-CoV-2 infection and lung disease in HLA-B*0702 *Ifnar1*^{-/-} mice.

A Experimental protocol for B to E. Mice were injected with SARS-CoV-2 N₁₀₄₋₁₁₃ vs DMSO (mock) on day 0 (complete Freund's adjuvant, CFA) and again on day 21 (incomplete Freund's adjuvant, IFA). Two weeks later, mice were challenged with SARS-CoV-2 B.1.351 (10⁵ PFU, IN), and tissues were collected at 3 days post-challenge. Mice/group: 8 (peptide-immunized) and 7 (mock). **B** ICS analysis of activated CD8⁺ T cells. Splenocytes were stimulated for 6 h with SARS-CoV-2 N₁₀₄₋₁₁₃ peptide, immunolabeled for cell surface markers, intracellular cytokines, and CD107a, and analyzed by flow cytometry. *N* = 7 and *N* = 8, respectively, for the mock and N₁₀₄₋₁₁₃ groups. **C** Representative H&E-stained sections of lungs. Blue arrows, bronchiolar epithelial cells (BEC); black arrows, epithelial cells within bronchioles. Sections were scored from 0 (least severe) to 5 (most severe) for standard histopathological features of SARS-CoV-2-induced lung disease. **D, E** RT-qPCR of SARS-CoV-2 genomic RNA in lungs, and representative

immunofluorescence of SARS-CoV-2 N protein (magenta) in lung sections with quantification of the N protein staining. In figure D, *N* = 7 and *N* = 8, respectively, for the mock and N₁₀₄₋₁₁₃ groups. In figure E, *N* = 9 and *N* = 7, respectively, for the mock and N₁₀₄₋₁₁₃ groups. **F** Experimental protocol for G to J. Mice were infected with OC43 (10⁹ GE, IN) vs PBS (naïve) and challenged with SARS-CoV-2 B.1.351 (10⁵ PFU, IN) 60–70 days later. Tissues were collected 3 days post-challenge. **G** ICS analysis of activated CD8⁺ T cells as described in B. Mice/group: 11 (OC43-infected) and 10 (naïve). **H, I** RT-qPCR of genomic SARS-CoV-2 RNA in lungs, and N protein staining in lung as described in D and E. Mice/group: 8 (OC43-infected) and 7-11 (naïve). **J** Lung histopathology and scoring as described in C. Mice/group: 8 (OC43-infected) and 11 (naïve). **B, D, E, G–I** Data pooled from 2 to 3 independent experiments and presented as the mean ± SEM. **C, J** Data pooled from 2 independent experiments and presented as violin plots. The means were compared using the two-sided Mann–Whitney test. Exact *P* values are indicated directly on the figure. Circles, individual mice.

Mice

For this study, we developed a mouse model in which HLA class I (HLA-B*0702 *Ifnar1*^{-/-}) or class II (HLA-DRB1*0101 *Ifnar1*^{-/-}) transgenic mice are infected sequentially with 1 of the 4 major seasonal human coronaviruses followed by SARS-CoV-2. Both transgenic mice were bred under pathogen-free conditions at La Jolla Institute for Immunology. The sex ratio for all experiments was approximately 1:1, and all experiments were started when mice were 5 to 7 weeks of age. For tissue collection, mice were euthanized by CO₂ inhalation. Blood samples were collected into serum collection tubes (Sarstedt) from a facial vein/cardiac puncture in ABSL2 or terminal eye bleeding in ABSL3. All samples were included in the analyses unless technical issues were evident, such as >50% cell mortality after cell isolation.

SARS-CoV-2 infections were performed in our high containment facility and OC43 infections in our biosafety level 2 infectious facility. All experiments were performed in strict accordance with recommendations set forth in the National Institutes of Health Guide for the Care and Use of Laboratory Animals and approved by the Institutional Animal Care and Use Committee at the La Jolla Institute for Immunology ABSL2 and ABSL3 (protocol number AP00001242). The study design was approved by the respective affiliated institutions of all authors.

Vaccination and infection

Mice were vaccinated IM (quadriceps) via electroporation with a minimally invasive device¹⁴² (BTX Agile Pulse system [47-0500 N] with a 4 × 4 × 5 mm needle array [47-0045]) with 25 μg of S, M, or N DNA vaccine and boosted 14 days later in the same manner. For vaccination with SARS-CoV-2 N₁₀₄₋₁₁₃ peptide, the peptide (250 μg) was diluted in PBS, homogenized in complete Freund's adjuvant (CFA), and injected IM (the site was gently massaged to facilitate dispersion of the peptide vaccine), and boosted 3 weeks later in the same manner homogenized in incomplete Freund's adjuvant (IFA). For the mock-vaccinated mice, peptide was replaced with DMSO.

Mice were infected IN with 10⁹ GE of OC43 (ATCC, VR-1558), 10⁴ PFU of SARS-CoV-2 MA10 (Leist et al., 2020), or 10⁵ PFU of SARS-CoV-2 B.1.351 (isolate HCoV-19/South Africa/KRISP-K005325/2020, NR-54009); both SARS-CoV-2 strains were obtained from BEI Resources (NIAID, NIH).

DNA vaccine constructs and detection of viral proteins

Plasmids encoding SARS-CoV-2 S, M, or N proteins (SARS-CoV-2/human/USA/WA-CDC-WA1/2020 isolate, GenBank MN985325.1) were synthesized using human codon optimization. Optimized DNA sequences were synthesized (GenScript), digested with KpnI and NotI, and cloned into pVAX1 under the control of human cytomegalovirus immediate-early promoter with a bovine growth hormone polyadenylation signal and kanamycin as a resistance marker. To increase efficiency of translational initiation, Kozak and IgE leader sequences were introduced. An empty pVAX1 vector served as a negative control.

For transfection, 293 T cells were seeded at 2 × 10⁵ cells/well in 24-well plates in DMEM supplemented with 10% fetal bovine serum (FBS), 1% penicillin–streptomycin, and 1% HEPES buffer, and grown to 70–80% confluence (37 °C, 5% CO₂). One hour before transfection, the supernatant was removed, 200 μl of Opti-MEM™ (Thermo Fisher Scientific) was added, and cell monolayers transfected with DNA vaccines or empty pVAX1 mixed with Lipofectamine® 2000 (1.5 μg/3 μL) per manufacturer's instructions. After 20 hours, cells were rinsed 3 times with PBS, and protein expression was assessed by immunofluorescence microscopy or flow cytometry.

For microscopy, monolayers were fixed with Cytofix (BD Biosciences) per manufacturer's instructions, permeabilized with 0.1% Triton X-100 (for S and N proteins) or 0.05% saponin (for M protein) in PBS (10 min, room temperature), blocked with 3% BSA in PBS (30 min, room temperature), and immunolabeled with mouse monoclonal antibodies (1 h, room temperature) against S protein (Thermo Fisher Scientific, MA5-35946, RRID AB2866558) or N protein (Absolute Antibody, Ab01691-3), or a polyclonal antibody against M protein (Prosci, 9157) diluted 1:500 in 0.1% Triton X-100/PBS. Monolayers were then washed 3 times with PBS, incubated (1 h, room temperature) with Alexa Fluor 488-conjugated goat anti-mouse IgG (Thermo Fisher Scientific, A11001) diluted 1:200 in 3% BSA/PBS, washed 3 times with PBS, and overlaid with a drop of ProLong™ Gold Antifade Mountant (Thermo Fisher Scientific). Images were captured with a Keyence BZ-X810 fluorescence microscope using with a Plan Fluor 20X/0.5 dry objective.

For flow cytometry, cell monolayers were trypsinized, fixed, permeabilized with Cytofix/Cytoperm (BD Biosciences), and incubated with the anti-N protein and secondary antibodies as described above (30 min, 4 °C). Cells were washed twice with Cytoperm containing 0.1% BSA and once with FACS buffer, and then resuspended in FACS buffer. Data were collected on an LSR II flow cytometer (BD Biosciences) and analyzed using FlowJo software.

Virus propagation and titration

OC43 was propagated for 9 days in HCT-8 cells cultured in RPMI supplemented with 10% FBS, 1% penicillin–streptomycin, and 1% HEPES buffer. The supernatant was collected and virus was concentrated using a gradient-free method with an Amicon Ultra-15 centrifugal filter unit (Millipore Sigma, UFC9100). Each virus batch was titrated, as described previously¹⁴³, by amplifying the M protein gene using genomic RT-qPCR and the following primers: Rev, 5'-AAT GTA AAG ATG GCC GCG TAT T-3'; Fwd, 5'-ATG TTA ACC TT TAA TTG AGG ACT AT-3' (IDT Integrated DNA Technologies). Cycling conditions were as follows: transcription initiation (48 °C, 30 min), PCR activation (95 °C, 10 min), and 45 cycles of amplification (95 °C for 15 s and 60 °C for 1 min). Viral RNA concentration was calculated using a standard curve composed of at least 4 100-fold serial dilutions of in vitro-transcribed OC43 RNA.

SARS-CoV-2 MA10 and B.1.351 were propagated for 3 days in Vero cells (ATCC, CCL81) cultured in Dulbecco's Modified Eagle's Medium

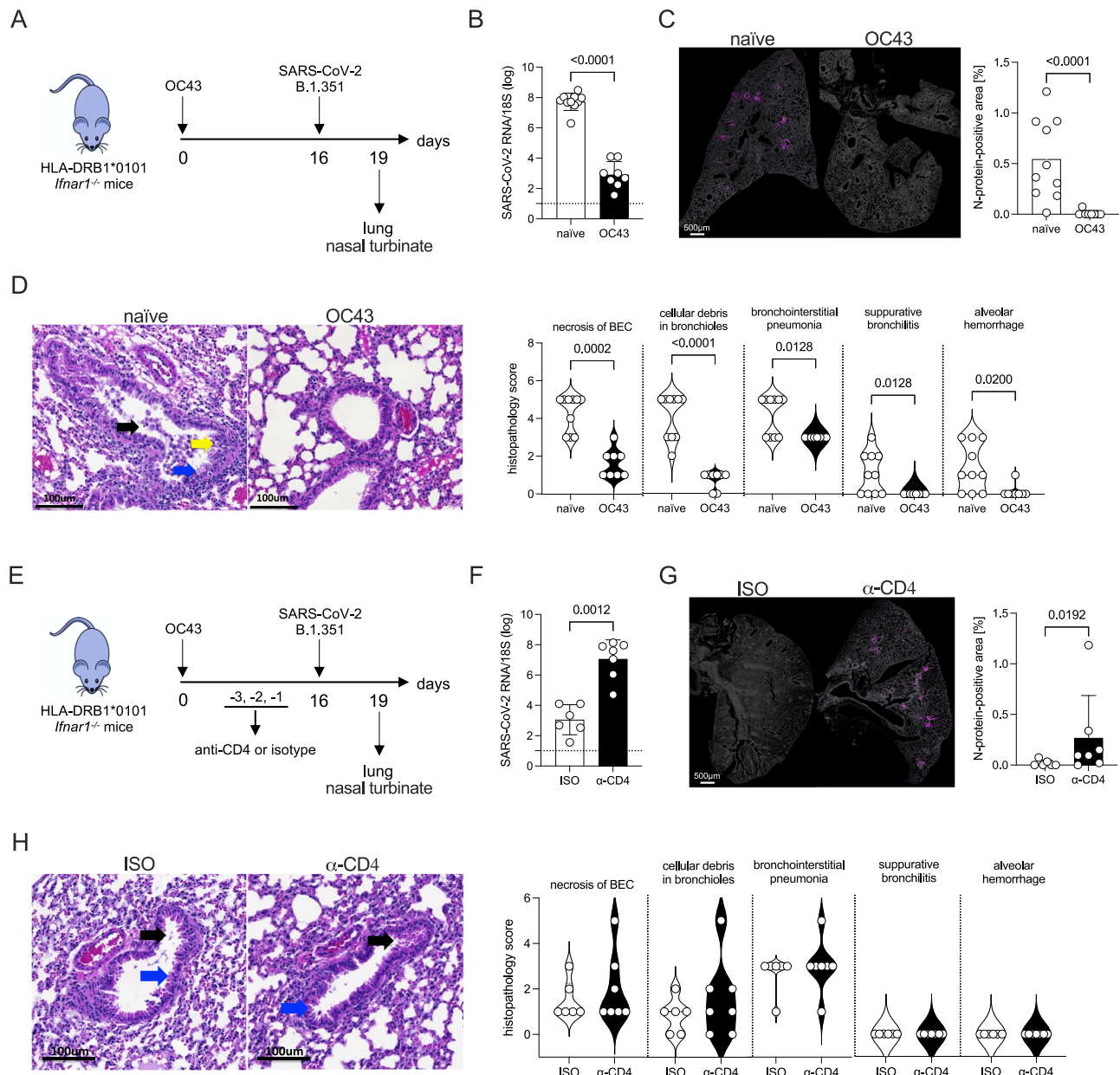


Fig. 6 | Protective effect of OC43 pre-exposure on SARS-CoV-2 infection and lung disease in HLA-DRB1*0101 *Ifnar1*^{-/-} mice. **A** Experimental protocol for B to D. Mice were infected with OC43 (10^5 GE, IN) *vs* PBS (naïve), challenged with SARS-CoV-2 B.1.351 (10^5 PFU) 16 days later, and lungs collected at 3 days post-challenge. **B**, **C** RT-qPCR of SARS-CoV-2 genomic RNA, and representative SARS-CoV-2 N protein (magenta) immunofluorescence in sections with quantification of the N protein staining. $N = 10$ and $N = 8$, respectively, for the naïve and OC43 groups. **D** Representative H&E-stained sections of lungs. Blue arrow, bronchiolar epithelial cells (BEC); black arrow, epithelial cells within bronchioles; yellow arrow, perivascular cuffing. Sections were scored from 0 (least severe) to 5 (most severe) for standard histopathological features of SARS-CoV-2-induced lung disease. $N = 10$ and $N = 8$, respectively, for the naïve and OC43 groups. **E** Experimental protocol for

F to **H**. Mice were infected with OC43 (10^5 GE, IN) *vs* PBS (naïve) and challenged with B.1.351 (10^5 PFU, IN) 16 days later. Mice were injected (IP) with CD4⁺ T cell-depleting antibody (α -CD4) *vs* isotype control antibody (ISO) once daily for 3 days before the challenge. Lungs were collected 3 days post-challenge. **F**, **G** RT-qPCR of genomic SARS-CoV-2 RNA in lungs, and N protein staining in the lung as described in B and C. $N = 6$ and $N = 7$, respectively, for the ISO and α -CD4 groups. **H** Lung histopathology and scoring as described for D. $N = 6$ and $N = 7$, respectively, for the ISO and α -CD4 groups. **B**–**D**, **F**–**H** Data, pooled from 2–3 independent experiments and presented as the mean \pm SEM or violin plots, were compared using the two-sided Mann–Whitney test. Exact P values are indicated directly on the figure. Circles, individual mice.

(Corning) supplemented with 10% FBS, 1% penicillin–streptomycin, 1% HEPES buffer, and 1% non-essential amino acids. The supernatant was harvested and titrated using a plaque assay¹⁴⁴. Briefly, 10-fold serially diluted viral supernatants were added to confluent Vero E6 cells (8×10^4 cells/well in 24-well plates; 2 h at 37 °C), supernatants removed, 1% carboxymethylcellulose medium added, and the cells incubated for 3 days. The cells were then fixed with 10% formaldehyde (1 h, room temperature) and stained with 0.1% crystal violet (20 min, room

temperature). Viral stocks were deep-sequenced by the La Jolla Institute for Immunology Sequencing Core.

Quantification of viral RNA in tissues

Organs were harvested, placed in 1 mL RNA/DNA shield (ZYMO Research, R1100-250) for 2 h to maintain high-quality RNA and inactivate the virus, and then transferred into RLT lysis buffer containing 1% 2-mercaptoethanol and homogenized (30 Hz, 3 min) using a Tissue

Lyser II (QIAGEN). Total RNA was extracted using a RNeasy Mini Kit (QIAGEN) and stored at -80°C . SARS-CoV-2 genomic E RNA and sub-genomic 7a RNA were quantified by RT-qPCR using the qScript One-Step qRT-PCR Kit (Quantabio). For the E gene, the following published primer sets¹⁴⁵ were used: Fwd, 5'-ACA GGT ACG TTA ATA GTT AAT AGC GT-3'; Rev, 5'-ATA TTG CAG TAC GCA CAC A-3'; and Probe, FAM-ACA CTA GCC ATC CTT ACT GCG CTT CG-BBQ. For the 7a gene, modified primer sets¹⁴⁶ were used: Fwd, 5'-TCC CAG GTA ACA AAC CAA CCA ACT-3'; Rev, 5'-AAA TGG TGA ATT GCC CTC GT-3'; and Probe, FAM-CAG TAC TTT TAA AAG ACC TT GCT CTT CTG GAA C-Tamra-Q. Viral RNA concentration was calculated using a standard curve derived from 4 10-fold serial dilutions of in vitro-transcribed SARS-CoV-2 RNA (from isolate USA-WA1/2020, ATCC NR-52347).

Production of recombinant SARS-CoV-2 S and N proteins

For SARS-CoV-2 S protein, HEK-293F cells were cultured to approximately 3×10^6 cells/mL, transfected with $3 \mu\text{g}/\text{mL}$ of Hexapro-Spike DNA; the S DNA was first mixed with $9 \mu\text{g}/\text{mL}$ of PEI-MAX (Polysciences), and shaken for 4–5 days (37°C , 80% humidity, 5% CO_2). When cell viability had decreased to 80%, the supernatant was harvested, centrifuged ($6000 \times g$, 20 min), mixed with Bioblock reagent (IBA Lifesciences, 2-0205-050; 1:300 v/v), stirred (15 min to overnight, 4°C), and centrifuged again ($6000 \times g$, 30 min) to remove Bioblock-conjugated biotin. From this clarified supernatant, S protein was purified by affinity chromatography using a Strep-Tactin column (IBA Lifesciences) on an AKTA purifier (GE Healthcare). Protein fractions were pooled and concentration estimated by UV absorbance at 280 nm. Tags were removed by addition of HRV-3C protease (10% w/w), and the digested protein further purified by size-exclusion chromatography using tandem Superose S6 Increase columns (GE Healthcare). The purified untagged S protein was concentrated using Vivaspin 500-10 K filters (Sartorius), aliquoted, flash-frozen in liquid nitrogen, and stored at -80°C .

Codon-optimized SARS-CoV-2 N was cloned into pET46 vector (Novagen) with an upstream hexahistidine tag followed by an enterokinase and tobacco etch virus (TEV) cleavage site. Plasmid (100 ng) was transformed by heat shock in Rosetta2 pLysS *E. coli* (Novagen), and starter cultures grown with 20 g/mL chloramphenicol and 100 g/mL ampicillin in 50 mL Luria-Bertani broth (LB) (37°C). After 14–16 hours, these starter cultures were used to inoculate 1 L LB cultures containing 100 g/mL ampicillin. When the optical density at 600 nm (OD_{600}) reached ~ 0.6 , protein production was induced by the addition of 0.5 mM isopropyl- β -thiogalactopyranoside followed by incubation (16–18 h, 25°C). Cells were then pelleted, resuspended in binding buffer (50 mM Tris-HCl, pH 8.0, 300 mM NaCl, and 30 mM imidazole) supplemented with 500 U of benzonase (Biotool, B16012) and protease inhibitors (AEBSF, E64, pepstatin A), and lysed using a Microfluidics M-110P microfluidizer. Cell debris was removed by centrifugation ($25,000 \times g$, 25 min) followed by supernatant filtration (0.22 μm pore size). His-coupled SARS-CoV-2 N protein was incubated with nickel-nitrilotriacetic acid beads (1 h), eluted in binding buffer containing TEV protease (1 mg/mL, 0.5% wt/wt) to cleave the His-tag, and dialyzed overnight in snakeskin dialysis tubing (3500 kDa pore size) in 50 mM Tris-Cl, pH 8.5, and 300 mM NaCl. The protein was further purified by size-exclusion chromatography using tandem Superose S6 Increase columns, concentrated using Vivaspin 500-10 K filters (Sartorius), aliquoted, flash-frozen in liquid nitrogen, and stored at -80°C .

N and S protein-binding IgG ELISAs

High-binding affinity 96-well plates (Costar) were coated overnight with $1 \mu\text{g}/\text{mL}$ of recombinant SARS-CoV-2 S or N protein or OC43 S protein (Sino Biological, 40607-V08B), and then blocked with 5% blotting-grade casein (Bio-Rad). The following steps were performed at room temperature. Mouse serum samples were diluted 3-fold from

1:30 to 1:810 (S protein) or 1:30 to 1:65,610 (N protein) in 1% BSA/PBS, and added to the coated wells (1.5 h). Plates were washed 3 times with PBS containing 0.05% Tween-20 (pH 7.4), incubated with a 1:5000 dilution of horseradish peroxidase-conjugated anti-mouse IgG polyclonal antibody (Jackson ImmunoResearch) in 1% BSA/PBS, and washed again. Color development was initiated by the addition of TMB substrate (Pierce), and the plates were then incubated in the dark (15 min). The reaction was stopped by the addition of 2 N sulfuric acid (Fisher Chemical), and OD_{450} was read immediately using a SpectraMax M2 microplate reader (Molecular Devices). The cutoff for positive reactivity was 2 standard deviations above the mean OD of negative control wells coated with antigen but lacking serum.

Flow cytometry and ICS assay

To generate single-cell lung leukocytes, lungs were cut into small pieces, digested with 1 mg/mL type I collagenase (Worthington) and 20 U/mL DNase I (Thermo Fisher Scientific) (30 min, 37°C), mechanically dissociated using a gentleMACS Octo Dissociator, filtered through a 70- μm cell strainer, and red blood cells lysed with ACK lysing buffer (Gibco). To generate single-cell splenocytes, spleens were gently mashed with a syringe plunger, filtered through a 70- μm cell strainer, and treated with ACK lysing buffer.

Splenocytes or lung leukocytes were placed in 96-well round-bottom plates at 2×10^6 cells/well in complete RPMI and stimulated with 10 $\mu\text{g}/\text{mL}$ of SARS-CoV-2 peptides (37°C). After 1 hour, Brefeldin A (BioLegend; 1:1000 dilution) and rat anti-mouse CD107a (Clone 1D4B, Biolegend) were added and the cells incubated for an additional 4 hours. Positive and negative controls were stimulated for the same time with Cell Stimulation Cocktail (eBioscience) or no stimulant, respectively. At the end of the 4-hour incubation, cells were stained with eFluor 455 (UV) viability dye (Invitrogen) and fluorophore-conjugated antibodies against mouse CD3 ϵ (Tonbo, clone 145-2C11), CD8 α (BioLegend, clone 53-6.7), CD4 (eBioscience, clone GK1.5), CD44 (BioLegend, clone IM7), and CD62L (BioLegend, MFL-14). Cells were then fixed and permeabilized with Cytotfix/Cytoperm and stained with fluorophore-conjugated antibodies against mouse IFN γ (Tonbo, clone XMGL2), TNF α (eBioscience, clone MP6-XT22), IL-2 (BioLegend, clone JES6-5H4), CD107a (Biolegend, clone 1D4B), IL-4 (Biolegend, clone 11B11), and IL-17A (Biolegend, clone TC11-18H10.1). Data were collected on an LSR Fortessa flow cytometer (BD Biosciences) and analyzed using FlowJo software.

IFN γ -ELISpot assay

Splenocytes or lung leukocytes, prepared as described above, were plated at 10^5 cells/well in 96-well flat-bottom plates (Immobilon-P; Millipore, MA) pre-coated with anti-mouse IFN γ antibody (clone AN18; Mabtech, Sweden) and incubated (20 h, 37°C) with 10 $\mu\text{g}/\text{mL}$ of SARS-CoV-2 peptide. Plates were processed as previously described¹⁴⁷, and spot-forming cells (SFCs) counted with an ELISpot reader (MABTech).

CD4 $^+$ T cell depletion

Mice were injected IP with CD4 $^+$ T cell-depleting antibody (BioXCell, clone GK1.5) or rat IgG2 isotype control antibody (BioXCell, clone LTF-2) (250 μg , IP) on days -3 , -2 , and -1 before SARS-CoV-2 challenge. Blood was collected before SARS-CoV-2 challenge from each mouse and analyzed by flow cytometry to validate CD4 $^+$ T cell depletion.

Peptide prediction, selection, and immunization

HLA-DRB1*0101- and HLA-B*0702-restricted SARS-CoV2 N, S, and M protein-derived T cell epitopes were identified as follows. Protein sequences for SARS-CoV-2/human/USA/WA-CDC-WA1/2020 isolate (GenBank MN985325.1) were accessed via the NCBI protein database. Using the Immune Epitope Database (www.iedb.org) website tools and the "IEDB-recommended" method selection, MHC class II or class I peptide binding affinity predictions were obtained for all non-

redundant 15-mer peptides that bind the HLA-DRB1*0101 allele or for all 8- to 11-mer peptides that bind the HLA-B*0702 allele. The resulting peptide lists were sorted by increasing consensus percentile rank and the top 1% selected (Tables 1 and 2), synthesized, purified to ≥95% purity by TC Peptide Lab (San Diego) using reverse-phase HPLC, and validated by mass spectrometry. Peptides were dissolved in DMSO for use.

HLA-DRB1*0101- and HLA-B*0702-restricted SARS-CoV2 proteome-derived T cell epitopes were searched on the NIAID Virus Pathogen Database and Analysis Resource (<https://www.viprbrc.org/>; accessed May 2, 2021) by querying the virus species name “severe acute respiratory syndrome-related coronavirus” from “human” hosts. We limited our search to epitopes identified by at least 1 of the following T cell assays: ELISpot, ICS, or MHC-binding. The resulting 37 predicted HLA-DRB1*0101 and HLA-B*0702 epitopes (Tables 3 and 4) were synthesized as crude material (1 mg scale) by TC Peptide Lab (San Diego).

Histopathology

Lungs were fixed with zinc formalin (24 h, room temperature) and transferred to 70% alcohol. Fixed lungs were embedded in paraffin using standard procedures, sliced into 4- μ m sections, stained with H&E using a Leica ST5020 autostainer, and imaged with a Zeiss AxioScan Z1 (40 \times 0.95 NA objective). Histopathological analysis was performed by a board-certified veterinary pathologist, who was blinded to group identity. Sections were scored (0–5) for 10 criteria for SARS-CoV-2-induced pneumonia, as seen in hamsters, macaques, and COVID-19 patients¹⁴⁸.

Statistical analysis

Data are expressed as the mean \pm standard error (SEM) and were analyzed with Prism software v9.1.1 (GraphPad Software). Differences between group means were analyzed by the Kruskal–Wallis test (> 2 groups), nonparametric Mann–Whitney test (2 groups), 2-way ANOVA followed by Sidak’s multiple comparisons test (> 2 groups, >1 variable), or one-way ANOVA with Dunnett’s post-hoc test. $P < .05$ was considered statistically significant.

Reporting summary

Further information on research design is available in the Nature Portfolio Reporting Summary linked to this article.

Data availability

All data supporting this study’s findings are included in the text, figures, supplementary material, and the source data provided in this paper. The complete dataset of immunofluorescence and histopathology images has been deposited in the repository: <https://doi.org/10.5281/zenodo.10397796>¹⁴⁹. Source data are provided in this paper.

References

- Noh, J. Y., Jeong, H. W. & Shin, E. C. SARS-CoV-2 mutations, vaccines, and immunity: implication of variants of concern. *Signal Transduct. Target. Ther.* **6**, 203 (2021).
- Andrews, N. et al. Covid-19 vaccine effectiveness against the omicron (B.1.1.529) variant. *New Engl. J. Med.* **386**, 1532–1546 (2022).
- Geers, D. et al. SARS-CoV-2 variants of concern partially escape humoral but not T-cell responses in COVID-19 convalescent donors and vaccinees. *Sci. Immunol.* **6**, eabj1750 (2021).
- Nasreen, S. et al. Effectiveness of COVID-19 vaccines against symptomatic SARS-CoV-2 infection and severe outcomes with variants of concern in Ontario. *Nat. Microbiol.* **7**, 379–385 (2022).
- Wratil, P. R. et al. Three exposures to the spike protein of SARS-CoV-2 by either infection or vaccination elicit superior neutralizing immunity to all variants of concern. *Nat. Med.* **28**, 496–503 (2022).
- Sakurai, A. et al. Natural history of asymptomatic SARS-CoV-2 infection. *New Engl. J. Med.* **383**, 885–886 (2020).
- Spudich, S. & Nath, A. Nervous system consequences of COVID-19. *Science* **375**, 267–269 (2022).
- Xie, Y., Bowe, B. & Al-Aly, Z. Burdens of post-acute sequelae of COVID-19 by severity of acute infection, demographics and health status. *Nat. Commun.* **12**, 6571 (2021).
- Xie, Y., Xu, E., Bowe, B. & Al-Aly, Z. Long-term cardiovascular outcomes of COVID-19. *Nat. Med.* **28**, 583–590 (2022).
- Guan, W. J. et al. Clinical characteristics of coronavirus disease 2019 in China. *New Engl. J. Med.* **382**, 1708–1720 (2020).
- Al-Aly, Z., Xie, Y. & Bowe, B. High-dimensional characterization of post-acute sequelae of COVID-19. *Nature* **594**, 259–264 (2021).
- Muscogiuri, G. et al. Low-grade inflammation, CoVID-19, and obesity: clinical aspect and molecular insights in childhood and adulthood. *Int. J. Obes.* **46**, 1254–1261 (2022).
- Ng, W. H. et al. Comorbidities in SARS-CoV-2 patients: a systematic review and meta-analysis. *mBio* **12**, e03647–20 (2021).
- Price-Haywood, E. G., Burton, J., Fort, D. & Seoane, L. Hospitalization and mortality among black patients and white patients with Covid-19. *New Engl. J. Med.* **382**, 2534–2543 (2020).
- O’Driscoll, M. et al. Age-specific mortality and immunity patterns of SARS-CoV-2. *Nature* **590**, 140–145 (2021).
- Klang, E. et al. Severe obesity as an independent risk factor for covid-19 mortality in hospitalized patients younger than 50. *Obesity (Silver Spring)* **28**, 1595–1599 (2020).
- Jin, J. M. et al. Gender differences in patients with COVID-19: focus on severity and mortality. *Front. Public Health* **8**, 152 (2020).
- Mateus, J. et al. Selective and cross-reactive SARS-CoV-2 T cell epitopes in unexposed humans. *Science* **370**, 89–94 (2020).
- Dykema, A. G. et al. Functional characterization of CD4+ T cell receptors crossreactive for SARS-CoV-2 and endemic coronaviruses. *J. Clin. Invest.* **131**, e146922 (2021).
- Woldemeskel, B. A. et al. CD4+ T cells from COVID-19 mRNA vaccine recipients recognize a conserved epitope present in diverse coronaviruses. *J. Clin. Invest.* **132**, e156083 (2022).
- Le Bert, N. et al. SARS-CoV-2-specific T cell immunity in cases of COVID-19 and SARS, and uninfected controls. *Nature* **584**, 457–462 (2020).
- Tan, H. X. et al. Adaptive immunity to human coronaviruses is widespread but low in magnitude. *Clin. Transl. Immunol.* **10**, e1264 (2021).
- Grifoni, A. et al. Targets of T cell responses to SARS-CoV-2 coronavirus in humans with COVID-19 disease and unexposed individuals. *Cell* **181**, 1489–1501.e1415 (2020).
- Ni, L. et al. Detection of SARS-CoV-2-specific humoral and cellular immunity in COVID-19 convalescent individuals. *Immunity* **52**, 971–977.e973 (2020).
- Peng, Y. et al. Broad and strong memory CD4(+) and CD8(+) T cells induced by SARS-CoV-2 in UK convalescent individuals following COVID-19. *Nat. Immunol.* **21**, 1336–1345 (2020).
- Weiskopf, D. et al. Phenotype and kinetics of SARS-CoV-2-specific T cells in COVID-19 patients with acute respiratory distress syndrome. *Sci. Immunol.* **5**, eabd2071 (2020).
- Kundu, R. et al. Cross-reactive memory T cells associate with protection against SARS-CoV-2 infection in COVID-19 contacts. *Nat. Commun.* **13**, 80 (2022).
- Lineburg, K. E. et al. CD8(+) T cells specific for an immunodominant SARS-CoV-2 nucleocapsid epitope cross-react with selective seasonal coronaviruses. *Immunity* **54**, 1055–1065.e1055 (2021).
- Braun, J. et al. SARS-CoV-2-reactive T cells in healthy donors and patients with COVID-19. *Nature* **587**, 270–274 (2020).
- Garcia-Jimenez, A. F. et al. Cross-reactive cellular, but not humoral, immunity is detected between OC43 and SARS-CoV-2

- NPs in people not infected with SARS-CoV-2: Possible role of cT(FH) cells. *J. Leukoc. Biol.* **112**, 339–346 (2022).
31. Westphal, T. et al. Evidence for broad cross-reactivity of the SARS-CoV-2 NSP12-directed CD4(+) T-cell response with pre-primed responses directed against common cold coronaviruses. *Front. Immunol.* **14**, 1182504 (2023).
 32. Diniz, M. O. et al. Airway-resident T cells from unexposed individuals cross-recognize SARS-CoV-2. *Nat. Immunol.* **23**, 1324–1329 (2022).
 33. Mesel-Lemoine, M. et al. A human coronavirus responsible for the common cold massively kills dendritic cells but not monocytes. *J. Virol.* **86**, 7577–7587 (2012).
 34. Gorse, G. J., Patel, G. B., Vitale, J. N. & O'Connor, T. Z. Prevalence of antibodies to four human coronaviruses is lower in nasal secretions than in serum. *Clin. Vaccine Immunol.* **17**, 1875–1880 (2010).
 35. Ellis, P., Somogyvari, F., Virok, D. P., Nosedá, M. & McLean, G. R. Decoding Covid-19 with the SARS-CoV-2 Genome. *Curr. Genet. Med. Rep.* **9**, 1–12 (2021).
 36. Loyal, L. et al. Cross-reactive CD4(+) T cells enhance SARS-CoV-2 immune responses upon infection and vaccination. *Science* **374**, eabh1823 (2021).
 37. Mateus, J. et al. Low-dose mRNA-1273 COVID-19 vaccine generates durable memory enhanced by cross-reactive T cells. *Science* **374**, eabj9853 (2021).
 38. Bacher, P. et al. Low-avidity CD4(+) T cell responses to SARS-CoV-2 in unexposed individuals and humans with severe COVID-19. *Immunity* **53**, 1258–1271.e1255 (2020).
 39. Augusto, D. G. et al. A common allele of HLA is associated with asymptomatic SARS-CoV-2 infection. *Nature* **620**, 128–136 (2023).
 40. Gouma, S. et al. Health care worker seromonitoring reveals complex relationships between common coronavirus antibodies and COVID-19 symptom duration. *JCI Insight* **6**, e150449 (2021).
 41. Mallajosyula, V. et al. CD8(+) T cells specific for conserved coronavirus epitopes correlate with milder disease in COVID-19 patients. *Sci. Immunol.* **6**, eabg5669 (2021).
 42. Bonifacius, A. et al. COVID-19 immune signatures reveal stable antiviral T cell function despite declining humoral responses. *Immunity* **54**, 340–354.e346 (2021).
 43. Zellweger, R. M., Prestwood, T. R. & Shresta, S. Enhanced infection of liver sinusoidal endothelial cells in a mouse model of antibody-induced severe dengue disease. *Cell Host Microbe* **7**, 128–139 (2010).
 44. Zellweger, R. M. et al. CD8+ T cells can mediate short-term protection against heterotypic dengue virus reinfection in mice. *J. Virol.* **89**, 6494–6505 (2015).
 45. Balsitis, S. J. et al. Lethal antibody enhancement of dengue disease in mice is prevented by Fc modification. *PLoS Pathog.* **6**, e1000790 (2010).
 46. Wen, J. et al. Dengue virus-reactive CD8(+) T cells mediate cross-protection against subsequent Zika virus challenge. *Nat. Commun.* **8**, 1459 (2017).
 47. Wen, J. et al. CD4(+) T cells cross-reactive with dengue and zika viruses protect against zika virus infection. *Cell Rep.* **31**, 107566 (2020).
 48. Regla-Nava, J. A. et al. Cross-reactive Dengue virus-specific CD8(+) T cells protect against Zika virus during pregnancy. *Nat. Commun.* **9**, 3042 (2018).
 49. Katzelnick, L. C. et al. Zika virus infection enhances future risk of severe dengue disease. *Science* **369**, 1123–1128 (2020).
 50. Katzelnick, L. C. et al. Antibody-dependent enhancement of severe dengue disease in humans. *Science* **358**, 929–932 (2017).
 51. Salje, H. et al. Reconstruction of antibody dynamics and infection histories to evaluate dengue risk. *Nature* **557**, 719–723 (2018).
 52. Fowler, A. M. et al. Maternally acquired zika antibodies enhance dengue disease severity in mice. *Cell Host Microbe* **24**, 743–750.e745 (2018).
 53. Gordon, A. et al. Prior dengue virus infection and risk of Zika: a pediatric cohort in Nicaragua. *PLoS Med.* **16**, e1002726 (2019).
 54. Rodriguez-Barraquer, I. et al. Impact of preexisting dengue immunity on Zika virus emergence in a dengue endemic region. *Science* **363**, 607–610 (2019).
 55. Pedroso, C. et al. Cross-protection of dengue virus infection against congenital zika syndrome, Northeastern Brazil. *Emerg. Infect. Dis.* **25**, 1485–1493 (2019).
 56. Sridhar, S. et al. Effect of dengue serostatus on dengue vaccine safety and efficacy. *New Engl. J. Med.* **379**, 327–340 (2018).
 57. Sharp, T. M. et al. Knowledge gaps in the epidemiology of severe dengue impede vaccine evaluation. *Lancet Infect. Dis.* **22**, e42–e51 (2022).
 58. Katzelnick, L. C., Bos, S. & Harris, E. Protective and enhancing interactions among dengue viruses 1-4 and Zika virus. *Curr. Opin. Virol.* **43**, 59–70 (2020).
 59. Valentine, K. M., Croft, M. & Shresta, S. Protection against dengue virus requires a sustained balance of antibody and T cell responses. *Curr. Opin. Virol.* **43**, 22–27 (2020).
 60. Ngono, A. E. & Shresta, S. Immune response to dengue and zika. *Annu. Rev. Immunol.* **36**, 279–308 (2018).
 61. Hassert, M., Brien, J. D. & Pinto, A. K. Mouse models of heterologous flavivirus immunity: a role for cross-reactive T cells. *Front. Immunol.* **10**, 1045 (2019).
 62. Gonzalez-Galarza, F. F. et al. Allele frequency net database (AFND) 2020 update: gold-standard data classification, open access genotype data and new query tools. *Nucleic Acids Res.* **48**, D783–D788 (2020).
 63. Solberg, O. D. et al. Balancing selection and heterogeneity across the classical human leukocyte antigen loci: a meta-analytic review of 497 population studies. *Hum. Immunol.* **69**, 443–464 (2008).
 64. Bastard, P. et al. Autoantibodies neutralizing type I IFNs are present in ~4% of uninfected individuals over 70 years old and account for ~20% of COVID-19 deaths. *Sci. Immunol.* **6**, eabl4340 (2021).
 65. Bastard, P. et al. Autoantibodies against type I IFNs in patients with life-threatening COVID-19. *Science* **370**, eabd4585 (2020).
 66. Koning, R., Bastard, P., Casanova, J. L., Brouwer, M. C. & van de Beek, D. with the Amsterdam UMCC-BI. Autoantibodies against type I interferons are associated with multi-organ failure in COVID-19 patients. *Intensive Care Med.* **47**, 704–706 (2021).
 67. Troya, J. et al. Neutralizing autoantibodies to type I IFNs in >10% of patients with severe COVID-19 pneumonia hospitalized in Madrid, Spain. *J. Clin. Immunol.* **41**, 914–922 (2021).
 68. Vazquez, S. E. et al. Neutralizing autoantibodies to type I interferons in COVID-19 convalescent donor plasma. *J. Clin. Immunol.* **41**, 1169–1171 (2021).
 69. Wang, E. Y. et al. Diverse functional autoantibodies in patients with COVID-19. *Nature* **595**, 283–288 (2021).
 70. Zhang, Q. et al. Inborn errors of type I IFN immunity in patients with life-threatening COVID-19. *Science* **370**, eabd4570 (2020).
 71. Elong Ngono, A. et al. Protective role of cross-reactive CD8 T cells against dengue virus infection. *EBioMedicine* **13**, 284–293 (2016).
 72. Weiskopf, D. et al. Immunodominance changes as a function of the infecting dengue virus serotype and primary versus secondary infection. *J. Virol.* **88**, 11383–11394 (2014).
 73. Weiskopf, D. et al. Insights into HLA-restricted T cell responses in a novel mouse model of dengue virus infection point toward new implications for vaccine design. *J. Immunol.* **187**, 4268–4279 (2011).
 74. Wen, J. et al. Identification of Zika virus epitopes reveals immunodominant and protective roles for dengue virus cross-reactive CD8(+) T cells. *Nat. Microbiol.* **2**, 17036 (2017).
 75. Vita, R. et al. The Immune Epitope Database (IEDB): 2018 update. *Nucleic Acids Res.* **47**, D339–D343 (2019).

76. Leist, S. R. et al. A mouse-adapted SARS-CoV-2 induces acute lung injury and mortality in standard laboratory mice. *Cell* **183**, 1070–1085.e1012 (2020).
77. Liu, Y. et al. The N501Y spike substitution enhances SARS-CoV-2 infection and transmission. *Nature* **602**, 294–299 (2022).
78. Pan, T. et al. Infection of wild-type mice by SARS-CoV-2 B.1.351 variant indicates a possible novel cross-species transmission route. *Signal Transduct. Target Ther.* **6**, 420 (2021).
79. Ferretti, A. P. et al. Unbiased screens show CD8(+) T cells of COVID-19 patients recognize shared epitopes in SARS-CoV-2 that largely reside outside the spike protein. *Immunity* **53**, 1095–1107.e1093 (2020).
80. Nguyen, T. H. O. et al. CD8(+) T cells specific for an immunodominant SARS-CoV-2 nucleocapsid epitope display high naive precursor frequency and TCR promiscuity. *Immunity* **54**, 1066–1082.e1065 (2021).
81. Schulien, I. et al. Characterization of pre-existing and induced SARS-CoV-2-specific CD8(+) T cells. *Nat. Med.* **27**, 78–85 (2021).
82. Sekine, T. et al. Robust T cell immunity in convalescent individuals with asymptomatic or mild COVID-19. *Cell* **183**, 158–168.e114 (2020).
83. Painter, M. M. et al. Rapid induction of antigen-specific CD4(+) T cells is associated with coordinated humoral and cellular immunity to SARS-CoV-2 mRNA vaccination. *Immunity* **54**, 2133–2142.e2133 (2021).
84. Dan, J. M. et al. Immunological memory to SARS-CoV-2 assessed for up to 8 months after infection. *Science* **371**, eabf4063 (2021).
85. Hicks, J. et al. Serologic cross-reactivity of SARS-CoV-2 with endemic and seasonal betacoronaviruses. *J. Clin. Immunol.* **41**, 906–913 (2021).
86. Saletti, G. et al. Older adults lack SARS CoV-2 cross-reactive T lymphocytes directed to human coronaviruses OC43 and NL63. *Sci. Rep.* **10**, 21447 (2020).
87. Nickbakhsh, S. et al. Epidemiology of seasonal coronaviruses: establishing the context for the emergence of coronavirus disease 2019. *J. Infect. Dis.* **222**, 17–25 (2020).
88. Killerby, M. E. et al. Human coronavirus circulation in the United States 2014–2017. *J. Clin. Virol.* **101**, 52–56 (2018).
89. Snyder, T. M. et al. Magnitude and dynamics of the T-cell response to SARS-CoV-2 infection at both individual and population levels. *medRxiv* <https://doi.org/10.1101/2020.07.31.20165647> (2020).
90. Tarke, A. et al. Comprehensive analysis of T cell immunodominance and immunoprevalence of SARS-CoV-2 epitopes in COVID-19 cases. *Cell Rep. Med.* **2**, 100204 (2021).
91. Saini, S. K. et al. SARS-CoV-2 genome-wide T cell epitope mapping reveals immunodominance and substantial CD8(+) T cell activation in COVID-19 patients. *Sci. Immunol.* **6**, eabf7550 (2021).
92. Quadeer, A. A., Ahmed, S. F. & McKay, M. R. Landscape of epitopes targeted by T cells in 852 individuals recovered from COVID-19: Meta-analysis, immunoprevalence, and web platform. *Cell reports. Medicine* **2**, 100312 (2021).
93. Nelde, A. et al. SARS-CoV-2-derived peptides define heterologous and COVID-19-induced T cell recognition. *Nat. Immunol.* **22**, 74–85 (2021).
94. Grifoni, A. et al. A sequence homology and bioinformatic approach can predict candidate targets for immune responses to SARS-CoV-2. *Cell Host Microbe* **27**, 671–680.e672 (2020).
95. Kared, H. et al. SARS-CoV-2-specific CD8+ T cell responses in convalescent COVID-19 individuals. *J. Clin. Invest.* **131**, e145476 (2021).
96. Ng, O. W. et al. Memory T cell responses targeting the SARS coronavirus persist up to 11 years post-infection. *Vaccine* **34**, 2008–2014 (2016).
97. Prakash, S. et al. Genome-wide B cell, CD4(+), and CD8(+) T cell epitopes that are highly conserved between human and animal coronaviruses, identified from SARS-CoV-2 as targets for pre-emptive pan-coronavirus vaccines. *J. Immunol.* **206**, 2566–2582 (2021).
98. Shen, Y et al. Ancestral origins are associated with SARS-CoV-2 susceptibility and protection in a Florida patient population. *bioRxiv* <https://doi.org/10.1101/2022.03.30.486345> (2022).
99. Keller, M. D. et al. SARS-CoV-2-specific T cells are rapidly expanded for therapeutic use and target conserved regions of the membrane protein. *Blood* **136**, 2905–2917 (2020).
100. Tan, A. T. et al. Early induction of functional SARS-CoV-2-specific T cells associates with rapid viral clearance and mild disease in COVID-19 patients. *Cell Rep.* **34**, 108728 (2021).
101. Crotty, S. T follicular helper cell differentiation, function, and roles in disease. *Immunity* **41**, 529–542 (2014).
102. Ueno, H., Banchereau, J. & Vinuesa, C. G. Pathophysiology of T follicular helper cells in humans and mice. *Nat Immunol.* **16**, 142–152 (2015).
103. Heide, J. et al. Broadly directed SARS-CoV-2-specific CD4+ T cell response includes frequently detected peptide specificities within the membrane and nucleoprotein in patients with acute and resolved COVID-19. *PLoS Pathog.* **17**, e1009842 (2021).
104. Karsten, H. et al. High-resolution analysis of individual spike peptide-specific CD4(+) T-cell responses in vaccine recipients and COVID-19 patients. *Clin. Transl. Immunol.* **11**, e1410 (2022).
105. Corey, L. et al. SARS-CoV-2 variants in patients with immunosuppression. *New Engl. J. Med.* **385**, 562–566 (2021).
106. Redd, A. D. et al. CD8+ T-cell responses in COVID-19 convalescent individuals target conserved epitopes from multiple prominent SARS-CoV-2 circulating variants. *Open Forum Infect. Dis.* **8**, ofab143 (2021).
107. Naranbhai, V. et al. T cell reactivity to the SARS-CoV-2 Omicron variant is preserved in most but not all individuals. *Cell* **185**, 1041–1051.e1046 (2022).
108. Keeton, R. et al. T cell responses to SARS-CoV-2 spike cross-recognize Omicron. *Nature* **603**, 488–492 (2022).
109. Gao, Y. et al. Ancestral SARS-CoV-2-specific T cells cross-recognize the Omicron variant. *Nat. Med.* **28**, 472–476 (2022).
110. GeurtsvanKessel, C. H. et al. Divergent SARS-CoV-2 Omicron-reactive T and B cell responses in COVID-19 vaccine recipients. *Sci. Immunol.* **7**, eabo2202 (2022).
111. Sun, J. et al. Generation of a broadly useful model for COVID-19 pathogenesis, vaccination, and treatment. *Cell* **182**, 734–743.e735 (2020).
112. McMahan, K. et al. Correlates of protection against SARS-CoV-2 in rhesus macaques. *Nature* **590**, 630–634 (2021).
113. Soresina, A. et al. Two X-linked agammaglobulinemia patients develop pneumonia as COVID-19 manifestation but recover. *Pediatr. Allergy Immunol.* **31**, 565–569 (2020).
114. Bange, E. M. et al. CD8(+) T cells contribute to survival in patients with COVID-19 and hematologic cancer. *Nat. Med.* **27**, 1280–1289 (2021).
115. Zhuang, Z. et al. Mapping and role of T cell response in SARS-CoV-2-infected mice. *J. Exp. Med.* **218**, e20202187 (2021).
116. Israelow, B. et al. Adaptive immune determinants of viral clearance and protection in mouse models of SARS-CoV-2. *Sci. Immunol.* **6**, eabl4509 (2021).
117. Rydzynski Moderbacher, C. et al. Antigen-specific adaptive immunity to SARS-CoV-2 in acute COVID-19 and associations with age and disease severity. *Cell* **183**, 996–1012.e1019 (2020).
118. Nesterenko, P. A. et al. HLA-A(*)02:01 restricted T cell receptors against the highly conserved SARS-CoV-2 polymerase cross-react with human coronaviruses. *Cell Rep.* **37**, 110167 (2021).

119. Le Bert, N. et al. Highly functional virus-specific cellular immune response in asymptomatic SARS-CoV-2 infection. *J. Exp. Med.* **218**, e20202617 (2021).
120. Tan, C. C. S. et al. Pre-existing T cell-mediated cross-reactivity to SARS-CoV-2 cannot solely be explained by prior exposure to endemic human coronaviruses. *Infect. Genet. Evol.* **95**, 105075 (2021).
121. Eggenhuizen, P. J. et al. Heterologous immunity between SARS-CoV-2 and pathogenic bacteria. *Front. Immunol.* **13**, 821595 (2022).
122. Low, J. S. et al. Clonal analysis of immunodominance and cross-reactivity of the CD4 T cell response to SARS-CoV-2. *Science* **372**, 1336–1341 (2021).
123. Sagar, M. et al. Recent endemic coronavirus infection is associated with less-severe COVID-19. *J. Clin. Invest.* **131**, e143380 (2021).
124. Humbert, M. et al. Functional SARS-CoV-2 cross-reactive CD4(+) T cells established in early childhood decline with age. *Proc. Natl Acad. Sci. USA* **120**, e2220320120 (2023).
125. Zhao, J. et al. Airway memory CD4(+) T cells mediate protective immunity against emerging respiratory coronaviruses. *Immunity* **44**, 1379–1391 (2016).
126. Poston, D. et al. Absence of severe acute respiratory syndrome coronavirus 2 neutralizing activity in pre-pandemic sera from individuals with recent seasonal coronavirus infection. *Clin. Infect. Dis.* **73**, e1208–e1211 (2021).
127. Ercanoglu, M. S. et al. No substantial preexisting B cell immunity against SARS-CoV-2 in healthy adults. *iScience* **25**, 103951 (2022).
128. Pinto, D. et al. Broad betacoronavirus neutralization by a stem helix-specific human antibody. *Science* **373**, 1109–1116 (2021).
129. Sun, X. et al. Neutralization mechanism of a human antibody with pan-coronavirus reactivity including SARS-CoV-2. *Nat. Microbiol.* **7**, 1063–1074 (2022).
130. Dacon, C. et al. Broadly neutralizing antibodies target the coronavirus fusion peptide. *Science* **377**, 728–735 (2022).
131. Low, J. S. et al. ACE2-binding exposes the SARS-CoV-2 fusion peptide to broadly neutralizing coronavirus antibodies. *Science* **377**, 735–742 (2022).
132. Anderson, E. M. et al. Seasonal human coronavirus antibodies are boosted upon SARS-CoV-2 infection but not associated with protection. *Cell* **184**, 1858–1864.e1810 (2021).
133. Ng, K. W. et al. Preexisting and de novo humoral immunity to SARS-CoV-2 in humans. *Science* **370**, 1339–1343 (2020).
134. Poston, D. et al. Absence of SARS-CoV-2 neutralizing activity in pre-pandemic sera from individuals with recent seasonal coronavirus infection. *medRxiv* <https://doi.org/10.1101/2020.10.08.20209650> (2020).
135. Premkumar, L. et al. The receptor binding domain of the viral spike protein is an immunodominant and highly specific target of antibodies in SARS-CoV-2 patients. *Sci. Immunol.* **5**, eabc8413 (2020).
136. Grifoni, A. et al. Prior dengue virus exposure shapes T cell immunity to Zika Virus in humans. *J. Virol.* **91**, e01469–17 (2017).
137. Wragg, K. M. et al. Establishment and recall of SARS-CoV-2 spike epitope-specific CD4(+) T cell memory. *Nat. Immunol.* **23**, 768–780 (2022).
138. Francis, J. M. et al. Allelic variation in class I HLA determines CD8(+) T cell repertoire shape and cross-reactive memory responses to SARS-CoV-2. *Sci. Immunol.* **7**, eabk3070 (2022).
139. Heitmann, J. S. et al. A COVID-19 peptide vaccine for the induction of SARS-CoV-2 T cell immunity. *Nature* **601**, 617–622 (2022).
140. Bastard, P. Why do people die from COVID-19? *Science* **375**, 829–830 (2022).
141. Minervina, A. A. et al. SARS-CoV-2 antigen exposure history shapes phenotypes and specificity of memory CD8 T cells. *medRxiv* <https://doi.org/10.1101/2021.07.12.21260227> (2022).
142. Choi, H. et al. Protective immunity by an engineered DNA vaccine for Mayaro virus. *PLoS Negl. Trop. Dis.* **13**, e0007042 (2019).
143. Vijgen, L. et al. Development of one-step, real-time, quantitative reverse transcriptase PCR assays for absolute quantitation of human coronaviruses OC43 and 229E. *J. Clin. Microbiol.* **43**, 5452–5456 (2005).
144. Mendoza, E. J., Manguiat, K., Wood, H. & Drebot, M. Two detailed plaque assay protocols for the quantification of infectious SARS-CoV-2. *Curr. Protoc. Microbiol.* **57**, ecpmc105 (2020).
145. Corman, V. M. et al. Detection of 2019 novel coronavirus (2019-nCoV) by real-time RT-PCR. *Euro Surveill.* **25**, 2000045 (2020).
146. Alexandersen, S., Chamings, A. & Bhatta, T. R. SARS-CoV-2 genomic and subgenomic RNAs in diagnostic samples are not an indicator of active replication. *Nat. Commun.* **11**, 6059 (2020).
147. Elong Ngono, A. et al. Mapping and role of the CD8(+) T cell response during primary Zika virus infection in mice. *Cell Host Microbe* **21**, 35–46 (2017).
148. Gruber, A. D. et al. Standardization of reporting criteria for lung pathology in SARS-CoV-2-infected hamsters: what matters? *Am. J. Respir. Cell Mol. Biol.* **63**, 856–859 (2020).
149. Alves, R. SOURCE_DATA_NCOMMS-23-38557B_part9 [Data set]. *Zenodo* <https://doi.org/10.5281/zenodo.10397796>, (2023).

Acknowledgements

We thank the Department of Laboratory Animal Care (Morag Mackay, Pascual Barajas, and Joseph Garza), the Department of Environmental Health and Safety (Dr. Laurence Cagnon and David Hall), and Flow Cytometry Core (Cheryl Kim) at the La Jolla Institute for Immunology for their assistance. We also thank Dr. Alessandro Sette at the La Jolla Institute for Immunology for providing HLA-B*0702 and DRB1*0101 *Irfar1*^{-/-} breeder mice. This study was funded by National Institutes of Health grants U19 AI142790-02S1 (to E.O.S. and S.S.) and U01 AI149644 (to R.S.B.), the GHR Foundation (to S.S. and E.O.S.), the Arvin Gottlieb Foundation (to S.S. and E.O.S.), and the Overton family (to S.S. and E.O.S.).

Author contributions

R.P.S.A., A.E.N., and S.S. conceived the study. R.P.S.A. and A.E.N. designed, performed, and analyzed the experiments. R.A., A.E.N., P.B.A.P., K.V., R.M., A.G., J.T., J.A.R.-N., M.N.N., E.M., S.L.-B., K.D., B.L., Z.M., S.M., N.S., and K.K. performed and analyzed experiments. S.R.L. and R.S.B. provided the MA10 virus strain. E.O.S. and S.S. obtained funding. S.S. supervised the research. R.P.S.A., A.E.N., and S.S. wrote the manuscript; other authors provided editorial comments.

Competing interests

The authors declare no competing interests.

Additional information

Supplementary information The online version contains supplementary material available at <https://doi.org/10.1038/s41467-024-45043-2>.

Correspondence and requests for materials should be addressed to Annie Elong Ngono or Sujana Shrestha.

Peer review information *Nature Communications* thanks Nimesh Gupta, Anthony Tan and the other, anonymous, reviewers for their contribution to the peer review of this work. A peer review file is available.

Reprints and permissions information is available at <http://www.nature.com/reprints>

Publisher's note Springer Nature remains neutral with regard to jurisdictional claims in published maps and institutional affiliations.

Open Access This article is licensed under a Creative Commons Attribution 4.0 International License, which permits use, sharing, adaptation, distribution and reproduction in any medium or format, as long as you give appropriate credit to the original author(s) and the source, provide a link to the Creative Commons licence, and indicate if changes were made. The images or other third party material in this article are included in the article's Creative Commons licence, unless indicated otherwise in a credit line to the material. If material is not included in the article's Creative Commons licence and your intended use is not permitted by statutory regulation or exceeds the permitted use, you will need to obtain permission directly from the copyright holder. To view a copy of this licence, visit <http://creativecommons.org/licenses/by/4.0/>.

© The Author(s) 2024

¹Center for Infectious Disease and Vaccine Research, La Jolla Institute for Immunology, La Jolla, CA, USA. ²Microscopy and Histology Core Facility, La Jolla Institute for Immunology, La Jolla, CA, USA. ³Department of Epidemiology, University of North Carolina at Chapel Hill, Chapel Hill, NC, USA. ⁴Histopathology Core Facility, La Jolla Institute for Immunology, La Jolla, CA, USA. ⁵Department of Microbiology and Immunology, University of North Carolina at Chapel Hill, Chapel Hill, NC, USA. ⁶Department of Medicine, Division of Infectious Diseases and Global Public Health, University of California, San Diego (UCSD), La Jolla, CA, USA. ⁷Present address: Department of Microbiology and Pathology, University Center for Health Science (CUCS), University of Guadalajara, Guadalajara 44340, Mexico. ✉ e-mail: aelong@lji.org; sujan@lji.org